APPLICATION OF PERIODIC OPERATION TO SULFUR DIOXIDE OXIDATION

Peter L. Silveston

Department of Chemical Engineering, University of Waterloo, Waterloo, Ontario, Canada N2L 3G1

Li Chengyue

Department of Chemical Engineering, Beijing University of Chemical Technology, Beijing 100029, China

Yuan Wei-Kang

Department of Chemical Engineering, East China University of Chemical Technology, Shanghai 201107, China

ADVANCES IN CHEMICAL ENGINEERING, VOL. 25 0065-2377/00 $30.00

Three different versions of periodic operation—composition modulation or catalyst flushing, flow direction switching, and flow interruption—have been tested on SO_2 oxidation over the past two decades. When applied to recovering sulfuric acid from SO_2 in plant emissions, improvements over steady-state operation are found for each version. However, among the different versions, only periodic switching of flow direction has been commercialized. This review examines plant data for flow direction switching as well as laboratory and modelling results for all versions of periodic operation. Comparing these versions one against the other for the same reaction provides a compact overview of possible industrial applications of periodic operations. Each version exploits a different process consideration and process improvements result from different physical and kinetic mechanisms.

I. Introduction

Sulfur dioxide oxidation is the essential catalytic reaction in the manufacture of one of the world's most important bulk chemicals: sulfuric acid. It is also a key step in processes now under consideration for removing sulfur from industrial stack gases. It is not surprising, then, that this reaction has been chosen to see if the emerging technique of periodic operation of chemical reactors would be useful commercially. What is surprising, however, is that three different types of periodic operation have been considered for this application: (1) periodic air blowing of the final stage of a multistage catalytic converter, (2) periodic reversal of flow direction in a single-stage converter, and (3) periodic interruption of liquid flow in a trickle-bed reactor. Research on these applications has attracted worldwide participation as Table I shows. There is a large literature on periodic flow reversal; only a few of the references are given. Others will be found in a review by Matros and Bunimovich (1996).

Sulfuric acid is produced commercially from a dust-free ore smelter off-gas or from a SO_2-rich gas stream obtained by burning sulfur. A multistage, near-adiabatic reactor employing trays of a granular, potassium-promoted vanadia catalyst is employed. The oxidation is highly exothermic, so heat must be removed. Various methods are used: heat exchange with a waste heat boiler or with the fresh gas feed, or cold gas injection. Cooling is usually carried out between stages, always prior to the last stage and frequently before the next-to-last stage. Conversion of SO_2 is equilibrium limited so, despite cooling prior to the final stage, SO_2 is not completely

TABLE I
GEOGRAPHIC DISTRIBUTION OF THE RESEARCH EFFORT ON THE APPLICATION OF PERIODIC OPERATION TO SO_2 OXIDATION

Type of periodic operation	Country	References
Periodic air blowing of the final stage of a multistage catalytic converter	Canada, Russia, USA	Briggs *et al.* (1977, 1978); Silveston and Hudgins (1981); Silveston *et al.* (1994; Strots *et al.* (1992)
Periodic reversal of flow direction in a single-stage converter	Russia, Bulgaria, China, Japan, USA	Boreskov *et al.* (1977); Boreskov and Matros (1984); Matros (1985, 1989); Sapundzhiev *et al.* (1990); Bunimovich *et al.* (1990); Isozaki *et al.* (1990); Snyder and Subramaniam (1993); Bunimovich *et al.* (1995); Xiao and Yuan (1996); Wu *et al.* (1996); Matros and Bunimovich (1996)
Periodic interruption of liquid flow in a trickle-bed reactor	Canada, Argentina, Russia, USA, Korea, Germany	Haure *et al.* (1989); Haure *et al.* (1990); Stegasov *et al.* (1992); Gangwal *et al.* (1992); Metzinger *et al.* (1994); Lee *et al.* (1995)

oxidized to SO_3. SO_3 leaving the multistage reactor is washed with quantitative capture of SO_3. Improvements to the current technology would be lower operating temperatures or other means of increasing SO_2 conversion in the reactor and lower-cost heat exchange.

Two of the three versions of periodic operation considered in this review were conceived to improve sulfuric acid production technology. Periodic air blowing is a method of reducing SO_2 emissions from sulfuric acid plants. The primary application of periodic flow reversal is to exhaust streams from metal smelters in which SO_2 concentrations are typically below 4.5 vol%. SO_2 can be oxidized with this periodic operation for large volumes of a low-temperature gas without requiring additional fuel or the use of expensive shell and tube heat exchangers. Periodic flow reversal also provides a declining temperature profile axially in the reactor that increases conversion when just a single reversible and highly exothermic reaction occurs. The third version, periodic interruption of liquid flow in a trickle bed, is aimed at removing parts-per-million amounts of SO_2 from stack gases while providing a moderately concentrated sulfuric acid product. It is one of several processes being considered for supplementing or even replacing lime addition to to coal-burning furnaces. Lime addition cannot meet the targets of 98% SO_2 removal that are now being sought.

Why are we comparing different versions of periodic operation for the same reaction? First of all, a comparison provides a compact review of this

type of operation without dealing in generalities or having to discuss details of different chemical systems. Process improvements achieved for SO_2 oxidation by each version typify what can be expected in applications to other reaction systems. Finally, this comparison demonstrates that the mechanisms that lead to process improvement are quite different for each version of periodic operation.

II. Air Blowing of the Final Stage of a Multistage SO_2 Converter

A. Experimental Studies

In 1973 Unni *et al.* (1973) published one of the first experimental studies of the periodic operation of a catalytic reactor. The authors chose SO_2 oxidation as their test reaction. A commercial catalyst containing 9.1 wt% V_2O_5, 10.1 wt% K_2O, and 0.45 wt% Fe_2O_3, supported on a diatomaceous earth, was employed, and experiments were run at 405°C and 1 bar so that conditions were similar to those found at the inlet to a commercial SO_2 converter. Catalyst size was reduced to 30/40 U.S. mesh, however, to avoid transport interference. Variables in the Unni study were cycle period, amplitude, and the time average feed composition. Both amplitude and the time average feed composition were expressed in terms of the $SO_2:O_2$ volume ratio. The remarkable finding was that SO_2 oxidation is excited at cycle periods measured in hours, as may be seen in Fig. 1. The largest rate enhancements were obtained at a time-average $SO_2:O_2$ ratio = 0.6 with an amplitude of 0.3 measured in terms of the $SO_2:O_2$ ratio. Higher and lower time average ratios (0.9 and 0.3) resulted in a significantly poorer performance, but this seems due to the lower amplitudes available at these averages. Symmetrical cycles were used by Unni *et al.*, but because ratios rather than concentrations were used, amplitudes for SO_2 and O_2 are not the same. Regardless of the time average $SO_2:O_2$ ratio, the largest enhancements were achieved at cycle periods between 4 and 6 h.

Strategies in which one reactant concentrations is held constant were examined in several runs at $\tau = 240$ min and are shown in the figure. These strategies appear to be comparable to variation of both reactants at a time average $SO_2:O_2$ ratio = 0.9, but variation of O_2 and N_2 holding SO_2 constant at a mean $SO_2:O_2$ ratio = 0.6 gave a value of Ψ less than half the value obtained when both reactants are cycled. Cycle amplitude with symmetrical forcing is important and it appears that a threshold amplitude between 0.1 and 0.2 as a $SO_2:O_2$ ratio exists. Too large an amplitude, which occurs

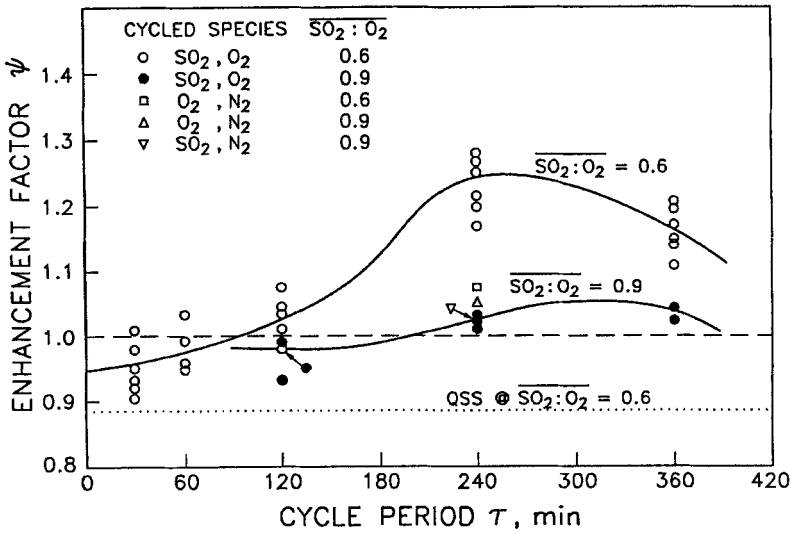

FIG. 1. Rate enhancement for SO_2 oxidation over a commercial promoted vanadia catalyst as a function of forcing period, time average feed composition as $SO_2:O_2$ ratio, and forcing manipulation (1 bar and 405°C, $s = 0.5$). (Figure adapted from Unni *et al.*, 1973, with permission of the authors.)

when one reactant is not present in the feed for a half cycle, diminishes the rate enhancement.

Briggs *et al.* (1977, 1978) attempted to apply the composition forcing used by Unni to decreasing emissions from SO_2 converters. They found, however, that with high levels of SO_3 in the feed no rate enhancement was achieved. Periodic blowing of the final stage in the converter to reduce the level of SO_3 on the catalyst offered a possible means to achieve higher rates, because SO_2 oxidation is inhibited by SO_3 at high SO_2 conversions under steady-state operation, so this approach was pursued.

The experiments undertaken by Briggs *et al.* (1977) and interpreted by Silveston and Hudgins (1981) explored the application of composition forcing to multistaged SO_2 converters. The same commercial catalyst employed by Unni *et al.* was chosen, but used in an integral reactor containing 30 g of 12/20 U.S. mesh particles. The initial experiments examined composition forcing at high conversion of a feed stream containing 12.4 vol% SO_2. Feed for the cycled stage was prepared in a separate converter containing a Pt/Al_2O_3 catalyst at 470°C. This converter, simulating the first three stages and operating at steady state, converted about 90% of the SO_2 in the feed to SO_3. Figure 2 shows the results obtained using symmetrical cycling with $\tau = 26$ min on the final converter stage. The 12.4 vol% SO_2 feed to the

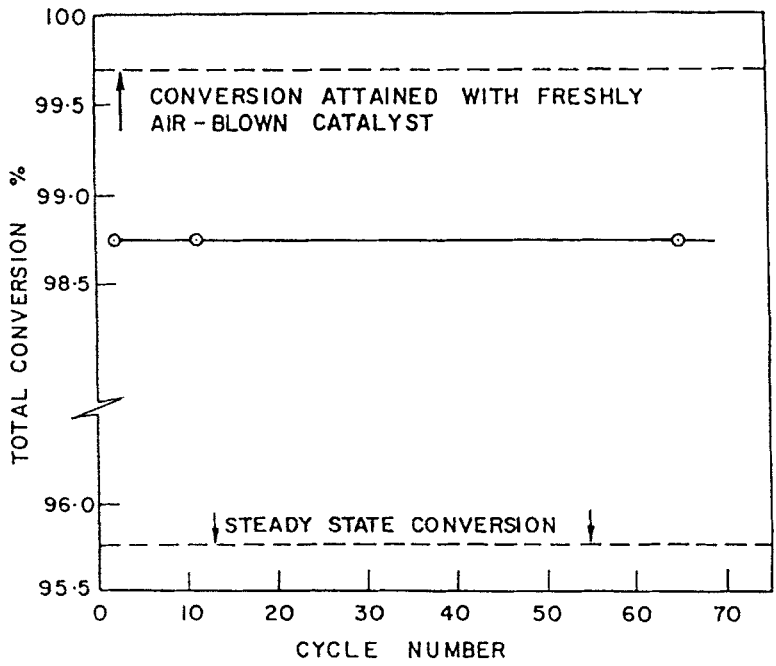

FIG. 2. Total SO_2 conversion in the SO_2-rich stream leaving the second reactor as a function of cycle number and type of reactor operation for a time average feed containing 12.4 vol% SO_2, T = 406°C. With composition forcing, measurement follows switch to the SO_3/SO_2 feed by 12 min. Reference lines (---) show limiting conversions for steady-state operation and under periodic forcing. (Figure adapted from Briggs *et al.*, 1977, with permission of the authors.)

steady-state preconverter is representative of acid plant feeds obtained by burning sulfur. When the catalyst bed operated at steady state, it raised the SO_2 conversion to 95.8%. The conversion under modulation, 12 min after introducing the SO_3:SO_2 mixture to the reactor, was 98.8%. The time average conversion in the half cycle was higher. Step change observations indicate that an even higher time average conversion could have been attained by shortening the half cycle, but the 12 min was dictated by the necessity of saturating the 97 wt% acid absorber with SO_2 before measurements could be made. Conversion in Fig. 2 is plotted against cycle number. The figure demonstrates that this high half-cycle conversion is maintained over some 30 h of operation. Only traces of SO_2 were detected leaving the vanadia catalyst bed 2 min after switching back to air. Consequently, no significant amounts of SO_2 are desorbed from the catalyst in the stripping step. Therefore, the figure represents the performance under composition modulation even though just half-cycle data are shown. It is notable that

the higher conversion achieved by modulation implies a 53% increase in catalyst activity.

The upper dashed line in Fig. 2 shows the initial conversion on switching in the step change experiment discussed earlier. It gives the limiting performance for final stage periodic air flushing at 406°C with feed typical of a sulfur burning acid plant. This conversion, 99.7%, exceeds slightly the equilibrium conversion of 99.4% calculated from the NBS tables of thermodynamic data at the temperature of the experiment.

Replacing air by either N_2 or O_2 did not affect the conversion obtained in the experiment just described. Consequently, the higher conversion does not result from catalyst reoxidation. It must be due solely to stripping SO_3 from the catalyst.

In order to explore composition modulation of the final stage of a converter further, Briggs *et al.* (1978) added a second integral reactor, also holding about 30 g of the vanadia catalyst. With the preconverter in place, this system was operated on a typical feed from sulfur burning, with a $SO_2 : O_2 : N_2$ composition in vol% of 10.8 : 15.2 : 74, and from a smelter effluent with a composition of 8.0 : 6.2 : 85.8. The cycled beds of vanadia catalyst were held in a fluidized sand bath at 401°C for the former feed and at 405°C for the latter one. The space velocity for both the air and the SO_3/SO_2 mixture was about 24 min^{-1} (STP). Table II summarizes the experimental results for the cycle periods tested.

SO_2 emitted from the modulated bed goes through a minimum after switching to the SO_3/SO_2 mixture. Lowest values are obtained 2 min after the composition change for the sulfur burning feed and they are about 8% of the steady-state emission, whereas for the smelter effluent feed, the lowest emission is about 13% of the steady-state value. Evidently, a cycle period of 4 to 5 min would be optimum for the conditions used, yielding a performance some 10% better than that shown at $\tau = 10$ in Table II.

The explanation of the delayed minimum in the SO_2 concentration is that data are for the combined streams emerging from the two parallel reactors, one of which is converting the $SO_2/SO_3/O_2$ mixture from the preconverter while the other is undergoing air blowing. The initially high SO_2 originates from the blowing step taking place in one of the beds. This drops with time in the half cycle and the SO_2 concentration approaches zero. The rising SO_2 concentration in the latter part of the half cycle comes from the other bed of the converter, where SO_2 reacts to form SO_3. Adsorption of SO_2 on the air-blown catalyst surface where a portion is oxidized to SO_3 keeps the SO_2 effluent from the active bed low. The trioxide is adsorbed (more strongly than SO_2) so this bed eventually saturates and the SO_2 concentration starts to climb.

A second group of experiments measured temperature variation in the

TABLE II
COMPOSITION CYCLING RESULTS

	Sulfur burning feed	Smelter off-gas feed
Feed: Mole ratio SO_2/O_2	0.709	1.30
Composition (mole frac.)		
SO_2	0.108	0.080
O_2	0.152	0.062
N_2	0.740	0.858
Bath temperature, final stage	401°C	405 ± 1°C
Mass of catalyst, final stage	25 g	23 g
Conversion (fractional)		
In preconverter	0.917	0.883
Final stage, steady stage	0.952	0.913
Final stage, cycling (mean value)		
for $\tau_{1/2}$ = 10 min	0.994	0.984
for $\tau_{1/2}$ = 20 min	0.992	0.981
for $\tau_{1/2}$ = 24 min	—	0.976
Equilibrium, steady state $(SO_2)^{eye}/(SO_2)^{steady}$ (mean molar ratio) from final stage	0.995[a]	0.987[a]
for $\tau_{1/2}$ = 10 min	0.122	0.184
for $\tau_{1/2}$ = 20 min	0.164	0.229
SO_2 concentration in gas leaving scrubber (SO_3-free) at steady state	6060 ppm	7790 ppm

[a] Calculated from NBS Table of Thermodynamic Data.

bed and the relative concentration of SO_3 leaving the bed during the two halves of a cycle (Briggs *et al.*, 1977). These measurements are shown in Fig. 3. The drop in temperature as SO_3 is stripped from the catalyst suggests either desorption from a melt phase or decomposition of a complex in that phase. Desorption and decomposition are endothermic. When the SO_3/SO_2 reactant mixture is reintroduced (Fig. 3b), the breakthrough behavior indicates SO_3 absorption. This is exothermic and it accounts for at least part of the temperature rise seen in the figure. Lack of symmetry in the feed and air flushing steps is notable because the duration of each step is the same. SO_3 desorption is incomplete after 13 min of air exposure, whereas the SO_3 breakthrough in the other cycle step takes less than 5 min. Temperature drop on SO_3 desorption is about 8°C, while the rise in the feed step is about 16°C. Oxidation of SO_2 when it is present in the feed step, however, explains this difference. The temperature rise after the minimum and the fall after the maximum temperatures in the cycle are consequences of placing the reactor in a fluidized sand bath held at 408°C. In an adiabatic reactor the temperature changes would be even larger.

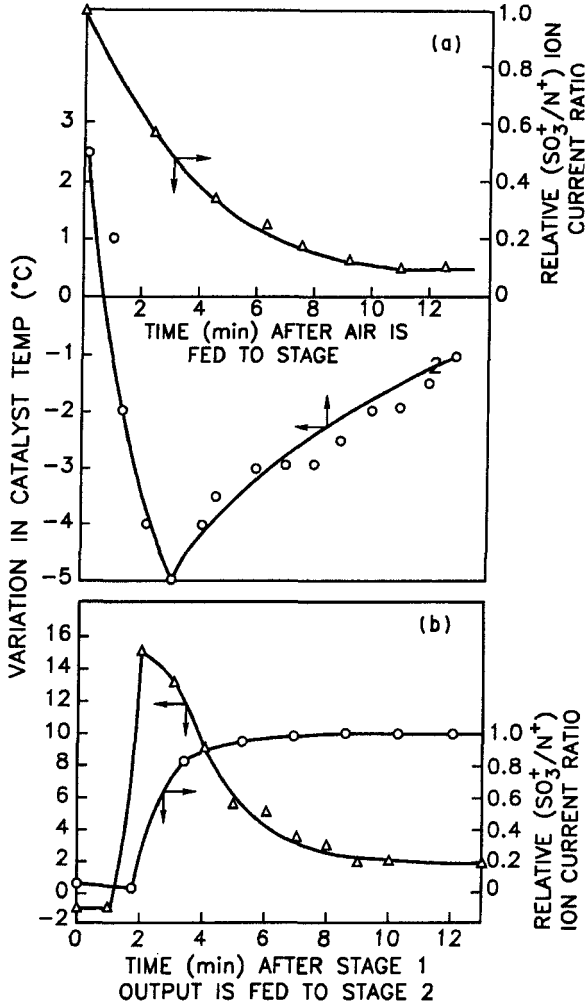

FIG. 3. Time variation of the catalyst bed temperature and the relative SO_3 signal in the stream leaving the cycled bed for composition forcing of the final stage of a SO_2 converter with an air stream and effluent from the previous stage: (a) half cycle with air feed, (b) half cycle with SO_3/SO_2 feed. Feed to the system contains 12.4 vol% SO_2, conversion in the first stage = 90% and $\tau = 26$ min, $s = 0.5$. (Figure adapted from Briggs *et al.*, 1977, with permission, © 1977 Elsevier Science Publishers.)

Figure 3 suggests that an unsymmetrical cycle with the duration of air flushing twice the duration of reactant feed would provide even greater reduction of SO_2 emissions. The drawback of unsymmetrical cycling is that more than two catalyst beds in parallel are needed. An alternative would

be to use a symmetrical cycle, but increase the airflow rate. This, however, would increase the loading on scrubbers in the acid plant. It is possible to avoid overloading the scrubbers by using the flushing air to burn sulfur. This scheme is shown in Fig. 4. It does not significantly affect the heat balance in the plant, but since the feed to the first bed of the converter will now contain a small amount of SO_3 there might even be a performance benefit, because low levels of SO_3 raise catalyst activity and the first stage is rarely equilibrium limited. Silveston and Hudgins (1981) used this scheme in their evaluation of the Briggs work. They concluded that the stiffest emission standards could be met at a cost below that for a double contact–double absorption plant for either a grass-roots situation or for a retrofit one when acid is produced by sulfur burning. The poorer performance of periodic air flushing with a smelter off-gas and the inability to recycle air probably mean that feed composition forcing is not attractive for producing acid from smelter off-gas. This exploratory work so far has failed to attract industrial interest despite its simplicity and apparent low cost.

SO_2 oxidation is one of the few reactions studied under periodic operation for which a mechanistic model is available. Moreover, a reactor model incorporating the mechanism and its kinetic model has been tested against forcing data. This modeling success means a model is available for exploring applications of periodic air flushing. An example of such an application where the objective is to examine different forcing strategies will be discussed in what follows.

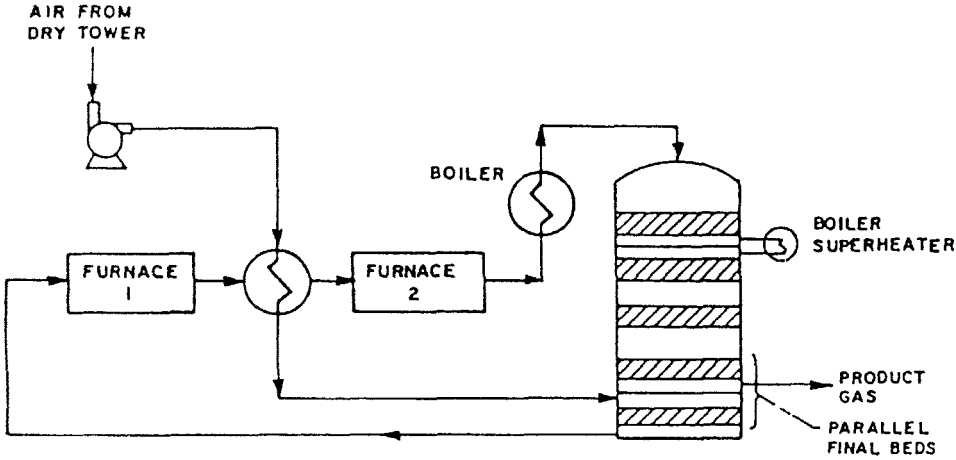

FIG. 4. Flow diagram of an SO_2 converter with periodic air flushing of the final catalyst stage and recycle of the air stream to the sulfur burner (in the diagram, air stripping of one of the final beds is shown). (Figure taken from Briggs *et al.*, 1978, with permission of the authors.)

B. Mechanistic Model

It has been known for decades that commercial potassium oxide–promoted vanadia catalysts function in a melt phase under reaction conditions and that SO_2 oxidation proceeds through a redox mechanism. Potassium oxide is converted to the pyrosulfate in the presence of SO_3 and this compound acts as a fluxing agent for vanadia. In recent years, a detailed mechanism has emerged (Balzhinimaev *et al.*, 1985, 1989). Potassium-promoted vanadia catalysts oxidize SO_2 through a redox cycle in which three different binuclear vanadium complexes participate. These are (1) an oxo complex with oxygen bridging two V atoms, (2) a sulfite complex in which SO_3 forms the bridge, and (3) a peroxo complex involving O_2 in the bridge. These complexes exist as oligomers in a melt with $K_2S_2O_7$ as the fluxing agent. The mechanism involves transformation of these complexes into one another through oxidation, SO_2 absorption, and the oxidation of SO_2 to SO_3. Fast side reactions involving $S_2O_7^{2-}$ remove vanadium from the melt phase by precipitation. A slow reduction step leads to V^{4+}, which is catalytically inactive. The mechanism is summarized in Table III. The bulk of the SO_3 produced comes from transfer between the V^{5+} complexes and does not involve a change in the coordination of vanadium. Dissolution of SO_3 in the melt is rapid as indicated in (1) of the table and can be treated as an equilibrium step. SO_3 is released from the melt by decomposition of the pyrosulfate. Oxygen enters the catalytic network through step (4), and its absorption in the melt may be rate controlling.

TABLE III
Vanadia Complex Transformation in the Balzhinimaev Mechanism[a]

$SO_3(g) + (SO_4^{2-})^m \xrightarrow{\text{rapid}} (S_2O_7^{2-})^m$	(1)[b]
$(V_2^{5+}O_2^{2-})^m + SO_2^{(m)} \underset{k_{-1}}{\overset{k_1}{\rightleftharpoons}} (V_2^{5+}O^{2-})^m + SO_3^m$	(2)
$(V_2^{5+}O^{2-})^m + SO_2^m \underset{k_{-2}}{\overset{k_2}{\rightleftharpoons}} (V_2^{5+}SO_3^{2-})^m$	(3)
$(V_2^{5+}SO_3^{2-})^m + O_2^m \underset{k_{-3}}{\overset{k_3}{\rightleftharpoons}} (V_2^{5+}O_2^{2-})^m + SO_3^m$	(4)
$(V_2^{5+}SO_3^{2-})^m \underset{k_{-4}}{\overset{k_4}{\rightleftharpoons}} (V_2^{4+})^m + SO_3^m$	(5)
$V_k + (S_2O_7^{2-}) \xrightarrow[K_{in}]{\text{rapid}} V_k^{in}$ (inactive form) $+ (S_2O_7^{2-})^m$	(6)

[a] m = molten or glass-like catalyst phase (species exists in this phase)

[b] All SO_3^m exists in the melt as $S_2O_7^{2-}$; thus, $C^m_{SO_3} = C^m_{S_2O_7^{2-}}$.

The kinetic model of Ivanov and Balzhinimaev (1987) and Balzhinimaev *et al.* (1989) assumes that the steps in the mechanism of Table III are elementary and that the active and inactive forms of the complexes are in equilibrium. Table IV presents the model. Parameters for the model are to be found in Table VI.

Application of the Balzhinimaev model requires assumptions about the reactor and its operation so that the necessary heat and material balances can be constructed and the initial and boundary conditions formulated. Intraparticle dynamics are usually neglected by introducing a mean effectiveness factor; however, transport between the particle and the gas phase is considered. This means that two heat balances are required. A material balance is needed for each reactive species (SO_2, O_2) and the product (SO_3), but only in the gas phase. Kinetic expressions for the Balzhinimaev model are given in Table IV.

C. Application to the Final Stage of SO_2 Converter with Composition Forcing

Silveston *et al.* (1994) use a one-dimensional plug flow model to represent the packed bed in the final stage. Because the intent of their work was to model the experiments of Briggs *et al.* discussed earlier, they allowed for heat loss or gain in the bench scale reactor used by Briggs through wall

TABLE IV
Kinetic Expression for the Balzhinimaev Model

$$\sum_k y_k + \sum_k y_k^{in} = 1 \qquad (7)^a$$

$$y_k^{in} = K_{in} C_{SO_3}^m y_k \qquad (8)$$

$$\Sigma y_k^{in} = \frac{K_{in} C_{SO_3}^m}{1 + K_{in} C_{SO_3}^m} \qquad (9)$$

$$r_1 = \frac{1}{1 + K_{in} C_{SO_3}^m} \left(k_1 P x_{SO_2} y_1 - \frac{k_{-1}}{K_H^3} C_{SO_3}^m y_2 \right) \qquad (10)$$

$$r_2 = \frac{1}{1 + K_{in} C_{SO_3}^m} (k_2 P x_{SO_2} y_2 - y_3) \qquad (11)$$

$$r_3 = \frac{1}{1 + K_{in} C_{SO_3}^m} \left(k_3 P x_{SO_2} y_3 - \frac{k_3}{K_H^3} C_{SO_3}^m y_1 \right) \qquad (12)$$

$$r_4 = \frac{1}{1 + K_{in} C_{SO_3}^m} \left(k_4 y_3 - \frac{k_{-4}}{K_H^3} C_{SO_3}^m y_4 \right) \qquad (13)$$

[a] Indices on y: 1, $(V_2^{5+}O_2^{2-})^m$; 2, $(V_2^{5+}O^{2-})^m$; 3, $(V_2^{5+}SO_3^{2-})^m$; 4, $(V_2^{4+})^m$.

transport terms employing overall bed-to-wall coefficients. They observed from comparison of the magnitude of terms in the balances that gas phase storage terms could be safely neglected. Table V gives their model. Note that these researchers incorporated reactions in the particle in their material balances rather than treating them as boundary conditions. Remaining boundary conditions and the initial conditions are given in the table. Each change of feed initiates a new solution so that two sets of initial conditions are needed: (1) $t = 0$, (2) $t = n\tau/2, n\tau, 3n\tau/2$, etc.

Parameters representing the catalyst bed were taken from Briggs *et al.* (1977, 1978); transport coefficients for heat and mass were calculated from well-established correlations, whereas the kinetic parameters came from measurements on Russian catalysts (Ivanov and Balzhinimaev, 1987) of about the same composition as the commercial catalyst used by Briggs. These parameters are collected in Table VI. The model used by Silveston *et al.* contained, therefore, no adjustable parameters.

Figure 5 gives the simulation results with the model given for the conditions used by Briggs *et al.* to obtain Fig. 3. Data points are shown in Fig. 5b, but not in 5a. Mass spectrometer readings were not calibrated, and only normalized data are shown in Fig. 3a. The simulation estimates the shape of the midbed temperature and the SO_3 vol% variations successfully. It also reproduces the initial bed temperature lag for the first minute after introduction of the SO_3/SO_2 reactant mixture (Fig. 5b), as well as the absence of a lag when air is introduced to the catalyst bed displacing the reactant mixture (Fig. 5a). The model also gives the slow adjustment of the bed temperature after the maximum and minimum temperatures, although the rates of cooling and heating are not correct. The most serious deficiency of the model is that it overestimates the temperature rise and drop by 15 and 8°C, respectively.

Integration of Eq. (6) for SO_2 in Table V estimates the conversion achieved. Simulation of periodic symmetrical switching between a reactant mixture and air gave an estimate of 99.4% at 12 min after the switch to the SO_3/SO_2 reactant mixture in reasonable agreement with the overall conversion of 98.8% measured by Briggs *et al.* (1977). With respect to model sensitivity, it was found that bed midpoint temperature was sensitive to the wall and gas to particle heat transfer coefficients. An extensive study of sensitivity, however, was not undertaken.

D. Application to an Isothermal Back-Mixed Reactor

Strots *et al.* (1992) undertook a study of composition forcing employing the Balzhinimaev model given in Table IV for the simplest reactor situation:

TABLE V

MODEL OF A NONADIABATIC PACKED BED REACTOR FOR SO_2 OXIDATION INCORPORATING THE BALZHINIMAEV MECHANISM[a]

Heat balance on the catalyst:

$$(1-\varepsilon_B)c_p^s\rho_{cat}\frac{\partial T_s}{\partial t} = \varepsilon_m(1-\varepsilon_B)H_3^{dis}\frac{\partial C_3^m}{\partial t} + \varepsilon_m(1-\varepsilon_B)s^v\sum r_jH_j + \varepsilon_m(1-\varepsilon_B)s^vH_{in}\frac{\partial \sum y_k^{in}}{\partial t} + h_pS_v(T-T_g) + h_wS_w(T_w-T_s) \tag{14}$$

Heat balance on gas phase:

$$0 = -u\rho_g c_p^g\frac{\partial T}{\partial z} + h_pS_v(T_g - T) + h_w^gS_w(T_w - T) \tag{15}$$

Mass balance on SO_3 in the melt phase:

$$\varepsilon_m(1-\varepsilon_B)\frac{\partial C_3^m}{\partial t} = k_mS_m\left(\frac{K_H^3Px_3^p}{1+K_H^3Px_3^p/C^o} - C_3^m\right) + \varepsilon_m(1-\varepsilon_B)s^v(r_1+r_2+r_4) - \varepsilon_m(1-\varepsilon_B)s^v\frac{\partial \sum y_k^{in}}{\partial t} \tag{16}$$

Mass balance on SO_3 in the particle void space:

$$0 = -k_mS_m\left(\frac{K_H^3Px_3^p}{1+K_H^3Px_3^p/C^o} - C_3^m\right) + k_p^3S_v(C_3^g - C_3^p) \tag{17}$$

Mass balances on SO_2 and O_2 in the particle void space:

$$0 = \varepsilon_m(1-\varepsilon_B)s^v\sum \nu_{ij}r_j + k_p^iS_v(C_i^g - C_i^p), \quad i = 1,2 \tag{18}$$

Gas phase mass balances on reactants:

$$0 = -u\frac{\partial C_i^g}{\partial z} + k_p^iS_v(C_i^p - C_i^g), \quad i = 1,2,3 \tag{19}$$

Number balances on vanadia complexes:

$$\frac{\partial y_k}{\partial t} = \Sigma\mu_{kj}r_j, \quad k = 1\text{–}4 \tag{20}$$

and

$$\Sigma y_k + \Sigma y_k^{in} = 1. \tag{21}$$

TABLE V (*Continued*)

Boundary conditions:

$$z = 0$$

$$(n-1)\tau < t < n\tau/2: \quad T = T^{\circ} \tag{22}$$

$$n = 1, 2, \ldots \qquad C_i = 0 \qquad i = 1\text{–}3$$

$$n\tau/2 < t < n\tau \qquad T = T^{\circ}$$

$$n = 1, 2, \ldots \qquad C_i = C_i^{\circ} \qquad i = 1, 2 \tag{23}$$

$$C_3 = 0$$

Initial conditions:

$$C_1 = 0 \qquad i = 1, 2, 3$$

$$t = 0; 0 \le z \le L: \quad C_3^{m} = 0$$

$$T_s = T = T^{\circ}$$

$$y_k, y_1^{in}, y_k^{in} = 0, k = 2, 3, 4$$

$$y_1 = 1$$

$$z \ge 0:$$

$$t = n\tau/2, n\tau \quad C_i^{g}(t^+) = C_i^{g}(t^-), C_i^{p}(t^+), = C_i^{p}(t^-), C_3^{m}(t^+) = C_3^{m}(t^-),$$

$$n = 1, 2, 3$$

$$y_k(t^+) = y_k(t^-), \qquad y_k^{in}(t^+) = y_k^{in}(t^-) \tag{24}$$

$$T(t^+) = T(t^-), \qquad T_s(t^+) = T_s(t^-)$$

[a] i = species index: 1 = SO_2, 2 = O_2, 3 = SO_3; j = reaction index: see Table III; k = complex index: see Table III.

a back-mixed reactor operating both isobarically and isothermally. These investigators also assumed equilibrium between the gas phase and the catalyst phase so heat and mass transport were neglected. With these assumptions, the equations in Table V simplify substantially to give

$$(\varepsilon_B(1 + \varepsilon_p(1 - \varepsilon_B)) + \varepsilon_m H_i RT)(dx_i/dt) \tag{25}$$
$$= ((x_i)_o - x_i)/t_s + (\varepsilon_m C_V RT/P)(S\nu_{ik} r_k),$$

$$i = SO_2, O_2, SO_3$$

$$dy_j/dt = \Sigma \mu_{jk} r_k \tag{26}$$

$$j = V_2^{5+}O_2^{2-}, V_2^{5+}O_2^{-}, V_2^{5+}SO_3^{2-}, V_2^{4+},$$

TABLE VI
MODEL PARAMETERS

Specific heats

$c_p^s = 0.21$ kcal/kg °C, $c_p^g = 1.08$ kcal/kg °C

Heat effects

$H_{in} = 26$ kcal/mol, $H_3^{dis} = 12$ kcal/mol

Solubility

$K_H^3 = 0.0372$ mol/cm^3 atm

Complex, sulfate, pyrosulfate concentrations

$s^v = 0.0024$ mol/cm^3, $C^o = 0.02$ mol/cm^3

Bed and catalyst properties

$\rho_{cat} = 264.7$ kg/m^3 $\rho_g = 0.25$ kg/m^3

$S_v = 3600$ m^{-1} $\varepsilon_B = \varepsilon_p = 0.4$

$\varepsilon_m = 0.20$ $u = 0.1$ m/s

Transport properties

$h_p = 0.528$ kcal/m^2 s °C $h_w = 2.2$ kcal/m^2 s °C

$h_{wg} = 0.5$ kcal/m^2 s °C $k_p = 0.315$ m/s

$k_m S_m = 6$ s^{-1}

where the index k signifies the reaction rates shown in Table IV. SO_3 is also stored in complexes present in the melt so that an additional term has to be added to the left side of Eq. (25). This term is

$$((\varepsilon_m C_V K_L H_{SO3} RT)/(1 + H_{SO3} P x_{SO3}((1/C_o) + K_L))^2)(dx_{SO3}/dt).$$

Strots *et al.* used the back-mixed reactor model to identify operating methods capable of improving the rate of this reaction for a given feed and set of operating conditions. They focused most of their effort on a forcing strategy using switching between an inert and the reaction mixture. The initial conditions expressing this strategy are

$$\begin{aligned} n\tau \le t \le (n + 1/2)\tau: &\quad (x_i)_o = 0 \\ n = 0, 1, 2, 3, \ldots & \\ (n + 1/2)\tau \le t \le (n + 1)\tau: &\quad (x_i)_o = 2(x_i)_o \end{aligned} \tag{27}$$

For their simulation of SO_2 oxidation, Strots *et al.* assumed $\varepsilon_B(1 + \varepsilon_p(1 - \varepsilon_B)) = 0.61$, $\varepsilon_m = 0.14$, $C_v = 0.002$, $C_o = 0.02$, $x_{SO3} = 0$ and $x_{SO2} =$

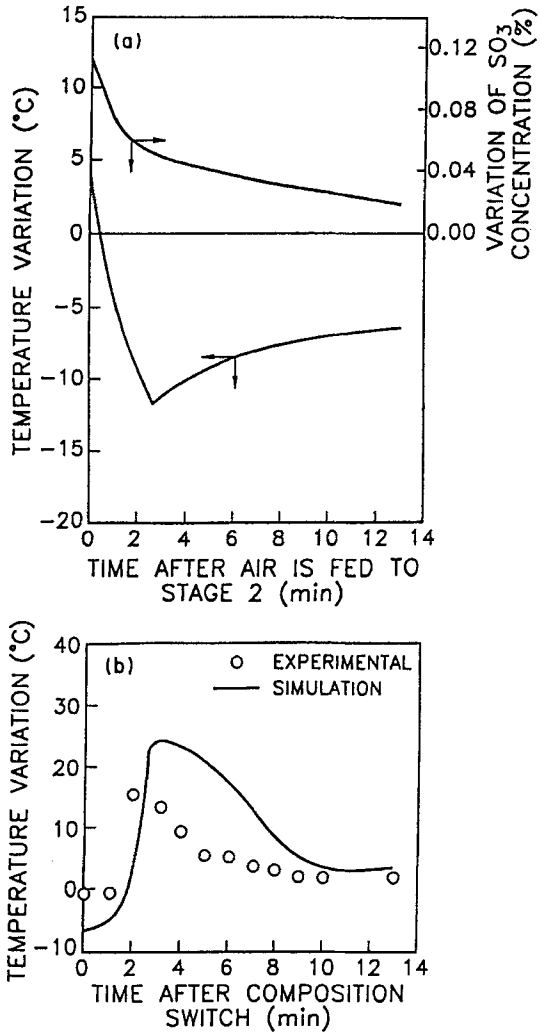

FIG. 5. Simulation of the composition forcing experiment of Briggs *et al.*, (1977) using the model of Table V with parameters from Table VI: (a) half cycle with air feed, (b) half cycle with SO_3/SO_2 feed. (Figure adapted from Silveston *et al.*, 1990, with permission, © 1990 VSP, Utrecht, The Netherlands.)

$x_{O2} = 0.1$. They examined the effect of temperature (673 to 798 K), space-time ($0.01 \leq \tau_s \leq 4$ s), and cycling strategy on rate enhancement. Resonance was observed for $\tau_s = 0.1$ s with $\Psi > 1$ for temperatures up to 770 K at a cycle period of about 1000 s. Above 770 K, $r_{qss} > r$ so that resonance disappeared. The quasi-steady-state rate, r_{qss}, decreased rapidly with de-

creasing temperature below 770 K, and this seemed to be responsible for the resonance observed.

Multiple resonance was observed at $T = 723$ K and $\tau_s = 0.01$ s. The enhancement, Ψ, exceeds 1 at a cycle period between 0.2 and 0.3 s and also at greater than 1000 s, although quasi steady state is also attained at about that period. Resonance also occurs at two different cycle periods at $\tau_s = 0.02$ s, Ψ is much smaller. As the space-time increases above 0.25 s, the rate enhancement becomes very small and the multiple resonance phenomenon seems to disappear.

The influence of cycling strategy on enhancement is given in Fig. 6 for $T = 723$ K and $\tau_s = 0.01$ s. Curve (3) shows forcing by switching between an inert and a reactant feed, that is, the strategy given by the initial conditions expressed in Eq. (27). This was the strategy used by Briggs *et al.* (1977,1978) in the experiments discussed earlier. Ψ is somewhat over 1.1. Curves (4) and (5) in Fig. 6 show the effect on enhancement of adding SO_3 to the reactor feed. To remain comparable to other curves in the figure, the condition $x_{SO2} + x_{SO3} = 1$ and $(x_{SO3} + x_{O2})/2 = 1$ is imposed. For $0.09 \leq x_{SO3}$ (corresponding to conversion of 90% of the SO_2 in feed to a preconverter to SO_3) the enhancement is negligible. However, the enhancement is over 30% for $x_{SO3} \geq 0.096$ (corresponding to 96% conversion of the SO_2 to SO_3) at a cycle

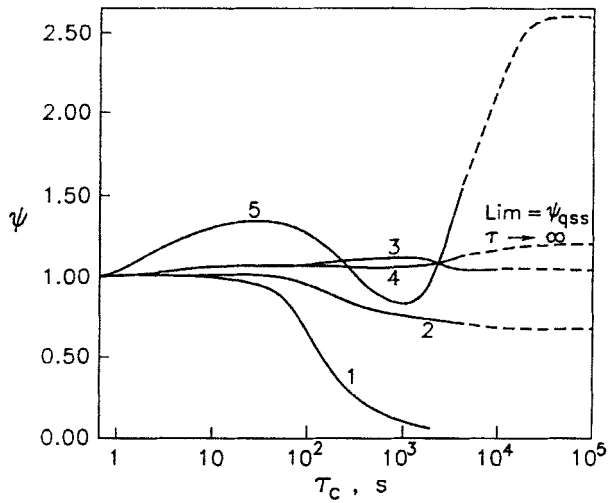

FIG. 6. Influence of the cycling strategy on the enhancement factor in a CSTR simulation at 723 K, $\tau_s = 0.1$ s. Curves: (1) SO_2 and O_2 concentration varied 180° out of phase, (2) only SO_2 concentration varied, (3) SO_2 and O_2 concentration varied in phase, (4) SO_3 present in the feed so that $x_{SO2} + x_{SO3} = 0.1$ and $(x_{O2} + x_{SO3})/2 = 0.1$ and $x_{SO3} = 0.09$, (5) as in (4) but with $x_{SO3} = 0.096$. (Figure taken from Strots *et al.*, 1992, with permission, © 1992 Elsevier Science Publishers.)

period between 20 and 100 s, and multiple resonance seems to arise. This result recalls Briggs' experiments on forcing the final stage of an SO_2 converter where enhancements of the order of 50% were observed at cycle periods in the range predicted by the Strots simulation.

If the SO_2 and O_2 concentrations are switched 180° out of phase so that SO_2 is absent from the reactor feed during one half cycle and O_2 is absent in the other half cycle, Fig. 6 shows that Ψ is less than 1 regardless of the cycle period. Forcing just the SO_2 concentration at a constant O_2 concentration also fails to enhance the rate of SO_2 oxidation in a back-mixed reactor. Even though the experiments of Unni *et al.* (1973), discussed earlier, were performed under isothermal conditions and differentially so that they could have been simulated by Strots' model, the strategy used by Unni was different from those investigated. Nevertheless, one of the experiments undertaken by Unni switched between a reactant mixture and a feed that did not contain SO_2. This experiment exhibited $\Psi < 1$. Strots' model predicts this observation.

Strots *et al.* (1992) studied the influence of model kinetics on enhancement under composition forcing and observed that Ψ significantly exceeds 1 when SO_3 desorbs faster than it decomposes because of the cycles involving vanadium complexes. This suggested raising the rate of oxidation by increasing the space velocity during the flushing half cycle to strip out more SO_3. Strots introduces a dissymmetry factor, D, to measure this velocity change, where D is the ratio of space velocities in the half cycles. Changing velocities was also mentioned discussing Briggs' study of forcing the final stage of a SO_2 converter by periodically flushing the bed in that stage with air. Strots noted that raising the space velocity by shortening the flushing portion of the cycle keeps the same mean feed composition. Strots and co-workers found that modulating the catalyst with a reactant mixture at a low space velocity and an inert stream at a high space velocity significantly increases the conversion attainable and may make it exceed the equilibrium limit that would be encountered in steady-state operation.

III. SO_2 Converters Based on Periodic Reversal of the Flow Direction

Development of this type of periodic operation has proceeded primarily at the Russian Academy of Science's Institute of Catalysis in Novosibirsk (Boreskov and Matros, 1984; Matros, 1985, 1989). Application to acid production has been discussed many times by Russian authors (see Matros, 1989).

Flow reversal can be exploited in various arrangements of one or more catalyst beds. The simplest scheme (Boreskov and Matros, 1984) uses a single catalyst bed and requires four quick-opening valves. For the best performance these valves should be leak-tight because of differing differential pressures across the valves in the on and off position. When flow occurs, as shown in Fig. 7, with cold feed entering the top of the bed, a front of decreasing temperature moves from the top of the bed to the bottom. After half a period, $\tau/2$, valves labeled "1" in the figure close and valves labeled "2" open. This changes the flow direction from downward to upwards and the temperature front now moves from the bottom to the top of the bed. This scheme is appropriate for reactant streams with a small adiabatic temperature rise (ΔT_{ad}). Problems are that the valves and associated piping may be subjected to large temperature variations during a cycle if ΔT_{ad} exceeds 80 to 100°C. In this case maximum bed temperature also may be high and catalyst damage could result. Of course, placing lift valves, which open only on flow, in the line can isolate the quick-opening,

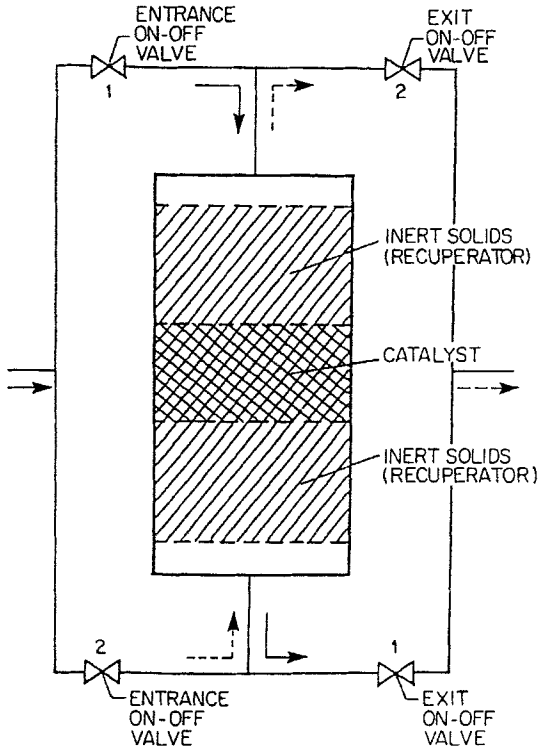

FIG. 7. Single-bed version of flow reversal with catalyst and inert packing zones. (Figure adapted from Matros, 1989, with permission, © 1989 Elsevier Science Publishers.)

leak-tight valves and substantially reduce the temperature variation they experience.

When $\Delta T_{ad} < 30°C$, heat recuperation is important. The outlet switching temperature will be low so the reaction contribution of the inlet and outlet regions is small. In this situation, inert packing with high heat capacity and low porosity can be used in place of catalyst. The variant is shown in Fig. 7.

Flow reversal performance is controlled weakly by the period τ. Flow reversal is an autothermal operation and as such exhibits parametric sensitivity. Greater stability can be ensured by the conventional expedient of providing cooling in the catalyst bed. It can also be done through bypassing part of the reactor effluent gas around the recuperator section.

A flow direction switch occurs at $\tau/2$ for a cycle period τ set by the plant operator, or it may be initiated by the reactor or recuperator outlet temperature. Startup of the flow-reversal system requires a heating device to bring the catalyst bed or at least the frontal portion up to ignition temperature. This temperature is about 350°C for SO_2 oxidation using conventional catalysts.

Catalyst circulation with gas flow always in the same direction is an alternative to periodic flow direction reversal. Circulating recuperator beds, usually with structured solids, have been used industrially for low-temperature applications for decades. If a catalytic material replaces the inert packing, most of the advantages of flow reversal can be retained. Although fast fluidization can be used for catalyst circulation, a rotating bed is the usual means of providing circulation. Rotating the catalyst avoids valve operation in a hostile environment, but brings with it new problems of moving solids at temperatures as high as 400°C and providing seals to minimize by passing.

A. Industrial Applications

As of 1990, seven industrial-scale plants were operating in Russia (Bunimovich *et al.*, 1990). The first plant started up in 1982. The design of these plants generally follows the schematic given in Fig. 7. Some employ an intermediate heat exchanger, but details have not been published. Designs are marketed around the world by several organizations.

Performance data have been published on most of the SO_2 oxidation flow reversal plants operating in Russia (Matros, 1989; Bunimovich *et al.*, 1990). These are summarized in Table VII. More than 14 years of operating data has been collected on the Krasnouralsk plant. The SO_2 concentration in the feed has varied considerably. Typically, during a working shift the variation is between 1 and 3%, but short-term variations have been much

TABLE VII

INDUSTRIAL-SCALE ACID PLANTS IN GREATER RUSSIA USING FLOW REVERSAL (BUNIMOVICH *et al.*, 1990)

No.	Enterprise, year of startup	Gas capacity, 10^3 m^3/h	SO_2 concentration (%)	Type of scheme	Cycle duration (min)	Conversion (%)	T_{max} in catalyst beds (°C)	Pressure drop (mm water)
1	Krasnouralsk Copper Smelter, 1982	40	1–2.5	Single-bed reactor	30–60	94–96	480–530	600–860
2	Mednogorsk Copper Smelter and Acid Plant, 1984	40	3–7	Reactor with intermediate heat removal	60–90	92–94	560–590	400–500
3	Krasnouralsk Copper Smelter, 1987	40	3–5	Reactor with intermediate heat removal	93–95	93–95	530–550	400–600
4	Ust-Kamenogorks Lead–Zinc Smelter, 1985	65	4–8	Reactor with damping bed	60–120	96–97.5	540–590	700–800
5	Alta Verdi Smelter, 1985	30	~4	DC/DA scheme with single bed, flow reversal used in second stage with SO_2 conc. 0–1%	80–100	95–96	520–560	~600
6	Pechenga-Nickel Smelter, 1987	90	1.5–3.5	Reactor with intermediate heat removal		95–96	480–520	600–800
7	Balkhas Copper Smelter, 1989	70	9–11	DC/DA scheme with single bed, flow reversal used in second stage with SO_2 conc. 0–1%		>99.5	460–480	

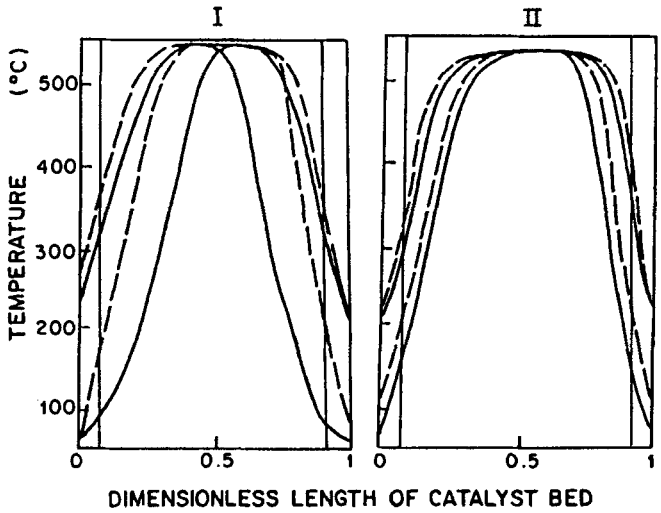

FIG. 8. Observed temperature profiles in a single, flow-reversal SO_2 oxidation reactor processing (I) 40,000 m^3/h, (II) 20,000 m^3/h of a smelter effluent containing 2.3 vol% SO_2. (Figure adapted from Matros, 1989, with permission, © 1989 Elsevier Science Publishers.)

larger. Hourly means ranged from 0.2 to 4.5%. Gas loading varies, too. Occasionally the reactor operates on half the loading given in the table (Matros, 1989; Bunimovich *et al.*, 1990). Figure 8 shows measured temperature profiles at extremes of gas loading for a feed gas containing 2–3% SO_2. Cycle period is about 25 min for the measurements in the figure. Feed enters the single-bed, reverse-flow reactor at temperatures between 50 and 70°C. Contiguous beds of inert packing are used at the reactor inlet and outlet as shown in Fig. 7. Flow direction switching is initiated by thermocouples at the top and bottom of the bed. At a low volumetric loading, the figure shows that about half the catalyst operates at virtually constant temperature. The largest temperature variations are confined to inert packing at the entrance and outlet. Increasing the volumetric loading twofold sharply narrows the constant temperature region (ca. 10% of the catalyst) and also raises the maximum temperature. Conversion is reduced.

Several pilot plants have been built to test periodic flow direction reversal. Pilot-scale reactors with bed diameters from 1.6 to 2.8 m were operated with flow reversal for several years. The units, described by Bunimovich *et al.* (1984, 1990) and Matros and Bunimovich (1996), handled 600 to 3000 m^3/h and operated with cycle periods of 15 to 20 min. Table VIII shows the performance of these plants for different feeds and potassium oxide promoted vanadia catalysts. The SVD catalyst was granular; the IK-1-4 was in the form of 5 (i.d.) × 10-mm cylinders, while the SVS catalyst was

TABLE VIII

PILOT PLANT PERFORMANCE ON DIFFERENT SO_2 FEED MIXTURES WITH COMPARISON TO MODEL SIMULATION (BUNIMOVICH *et al.*, 1990)

No.	Range of input SO_2 conc. (%)	Approx. O_2 conc. (%)	Catalyst type	Bed height (m)	Linear velocity (m)	Cycle duration (min)	Conversion (%)	Max. temp. (°C)	ΔP (mm water)	Assumed SO_2 (%)	Calc. conversion (%)	Calc. T_{max} (°C)	Calc. ΔP (mm water)
1	0.70–0.85	10	SVS	2.7									
			SVD		0.41	20	96–97	450	300	0.8	98.0	484	320
2	0.9–1.0	10	SVS	2.7	0.36	20	95–96	450	260	0.95	97.7	494	250
			SVD										
3	1.2–1.3	10	SVS	2.7	0.20	20	95–96	460	80–100	1.2	97.0	493	85
			SVD										
4	1.6–1.8	10	IK-1-4	2.0	0.23	30	94–95	500–510	200	1.7	95.6	527	160
5	2.1–2.6	11	IK-1-4	2.0	0.23	30	91–94	540–550	200	2.3	92.3	560	194
6	3.0–3.5	12.5	IK-1-4	2.0	0.25	25	90–93	590	280	3.2	90.0	596	230
7	3.1–3.3	12.5	SVS	2.7									
			SVD	1.7	0.20	50	93–94	540–550	80–100	3.2	91.0	580	95
8	3.1–3.3	12.5	SVD_{exp}	4.6	0.20	50	92–95	520	10–20	3.2	92.5	560	6
9	4.0–4.5	12.5	SVD_{exp}	1.7	0.13	30–40	90–92	580	10–15	4.2	90	588	12
10	5.9–6.1	15	SVD_{exp}	1.7	0.06	120	90–93	580	10–15	6	92.6	582	2
11	5.9–6.3	14.7	SVD	0.85	0.07	120	85–87	630–640	—	6	91.6	600	17
12	8.3–8.6	12.6	SVD_{exp}	1.75	0.06	120	85	610	—	8.4	86.2	612	2

25 (i.d.) × 50-mm hollow cylinders with a 2.6-mm wall thickness. Inlet temperatures were 30 to 50°C.

Table VIII demonstrates the inverse relationship of conversion to SO_2 concentration in the feed that is a consequence of applying flow reversal to SO_2 oxidation using a single reactor. As the SO_2 concentration in the table moves from 0.8 to over 8 vol%, the conversion drops from 96–97% down to 85%. At the same time, the maximum bed temperature changes from 450 to 610°C. For an equilibrium-limited, exothermic reaction, this behavior is explained by variation of the equilibrium conversion with temperature.

Xiao and Yuan (1996) also published pilot-plant measurements. These investigators employed a bypass stream from a full-scale acid plant. Their reactor consisted of three stages, each 800 mm in diameter and packed to a depth of 500 mm with a commercial Type S101 catalyst. Some cooling was provided after the first and second stages to minimize peak temperatures in the bed. Experiments were conducted with a feed gas containing about 8 vol% SO_2. Briggs *et al.* (1977, 1978) also used a feed of this composition in their experiments on periodic air blowing of the final stage of an SO_2 converter. Operating at a superficial velocity of 0.07 m/s, Xiao and Yuan report 77 to 80% conversion and a maximum bed temperature of about 640°C. Temperature profiles for upflow and down flow just before switching of the flow direction are shown in Fig. 9 for a cycle period of 120 min after the system has become cyclically invariant. The profiles are nearly symmetrical. The effect of interstage cooling is clearly seen. The curious "M" shape of the profiles appears to be due to completion of the reaction in the first stage as the temperature profile in the second stage varies by just 20°C. The temperature rise in the third stage is largely a "ghost" of the previous half cycle. Increasing the flow rate by about 40% had little effect on conversion and peak bed temperatures, but had a large effect on the contribution of cooling, thereby increasing the temperature in the second bed.

Isozaki *et al.* (1990) describe a double contacting-double absorption process utilizing flow reversal in both contacting stages. Figure 10 is a schematic flow diagram of the Hitachi Zosen design. The Isozaki paper gives performance details for a pilot plant operated in Saganoseki, Japan, in 1988. The first stage plant was designed to process 3000 to 3600 Nm^3/h of an acid plant feed containing 5–9 vol% SO_2 and 8–14 vol% O_2 available at 50 to 65°C. It achieved an 85 to 90% SO_2 conversion using a 50- to 60-min flow reversal cycle. The second stage operated on a feed with a SO_2 content of about 0.5 to 1.5 vol%. Intermediate cooling was not required as the figure shows. Initial tests on this plant at 3000 Nm^3/h showed conversions of 94 to 96% depending on the SO_2 concentration in the feed. Cycle periods

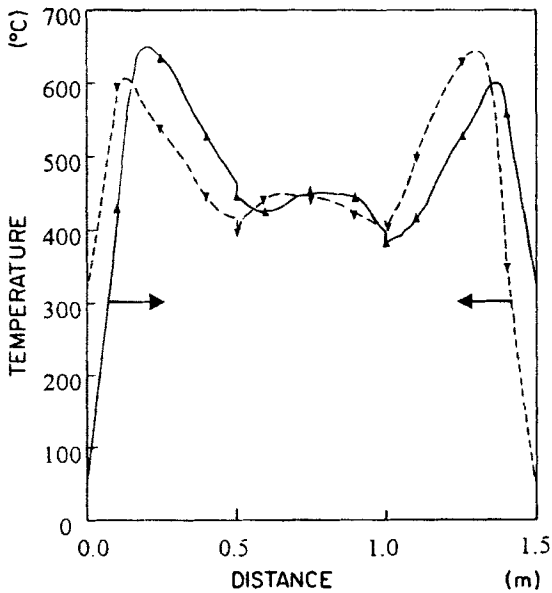

FIG. 9. Invariant cycling state temperature profiles for a three-stage, 800 mm diameter pilot plant SO_2 converter with interstage cooling. Profiles were measured just before switching of the flow direction and are for SO_2 at 7.6 vol% and a superficial velocity of 0.07 m/s. Catalyst was a commercial potassium-promoted vanadia, Type S101. (Figure adapted from Xiao and Yuan, 1996, with permission of the authors.)

varied between 20 and 36 min, increasing with higher SO_2 content in the feed. Operating both stages together would bring SO_2 conversion to just over 99.5%.

Application of flow reversal is particularly attractive for the second stage of a double absorption system, according to Matros (1985, 1986, 1989). A conventional first stage results in a feed gas for the second stage containing 0.5 to 1.0 vol% SO_2. At this level, maximum bed temperature will be under 500°C; temperature drops toward the outlet, so conversion of about 96% of the SO_2 entering the stage is possible. Over two stages, conversion reaches 99.6%. This agrees well with the Japanese results just mentioned. Two full-scale plants using flow reversal in the second stage have been operating in Russia since 1989 (Table VII).

B. EXPERIMENTAL RESULTS

Results for bench-scale flow-reversal units operated in Russia (Boreskov *et al.*, 1982: Matros, 1989) and China (Wu et al., 1996; Xiao and Yuan,

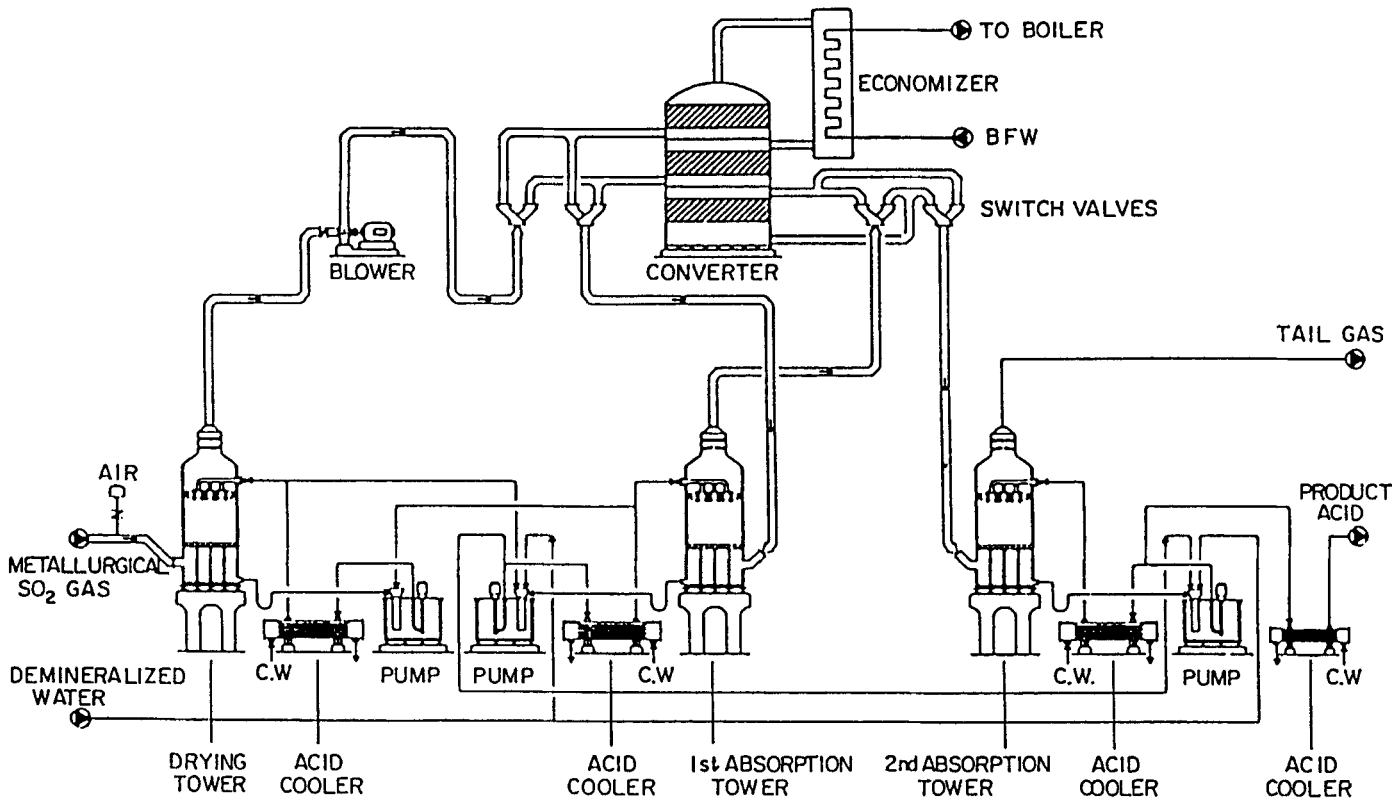

FIG. 10. Schematic flow sheet of the Hitachi Zosan DC/DA Acid Plant using two-stage flow reversal. (Figure adapted from Isozaki *et al.*, 1990, with permission, © 1990 VNU Science Publishers, Utrecht, Tokyo.)

1996) have been published. The experimental system used by Xiao and Yuan (1996) appears in Fig. 11. The reactor was 32 mm (i.d.) × 1100 mm and was packed with a Type S101 potassium-promoted vanadia catalyst to a depth of 900 mm. Inert packing, 100 mm, was placed above and below the catalyst. Wu *et al.* (1996) used the same commercial catalyst but employed a 50 mm (i.d.) × 4000 mm reactor, about half full of catalyst. By contrast, Russian researchers used a 175 mm (i.d.) × 1300 mm reactor. Development of the temperature profile after a switch in the direction of flow is shown in Fig. 12 for stationary, reproducible operation of a 2 m deep converter bed (Wu et al., 1996). Results for different SO_2 concentrations, superficial

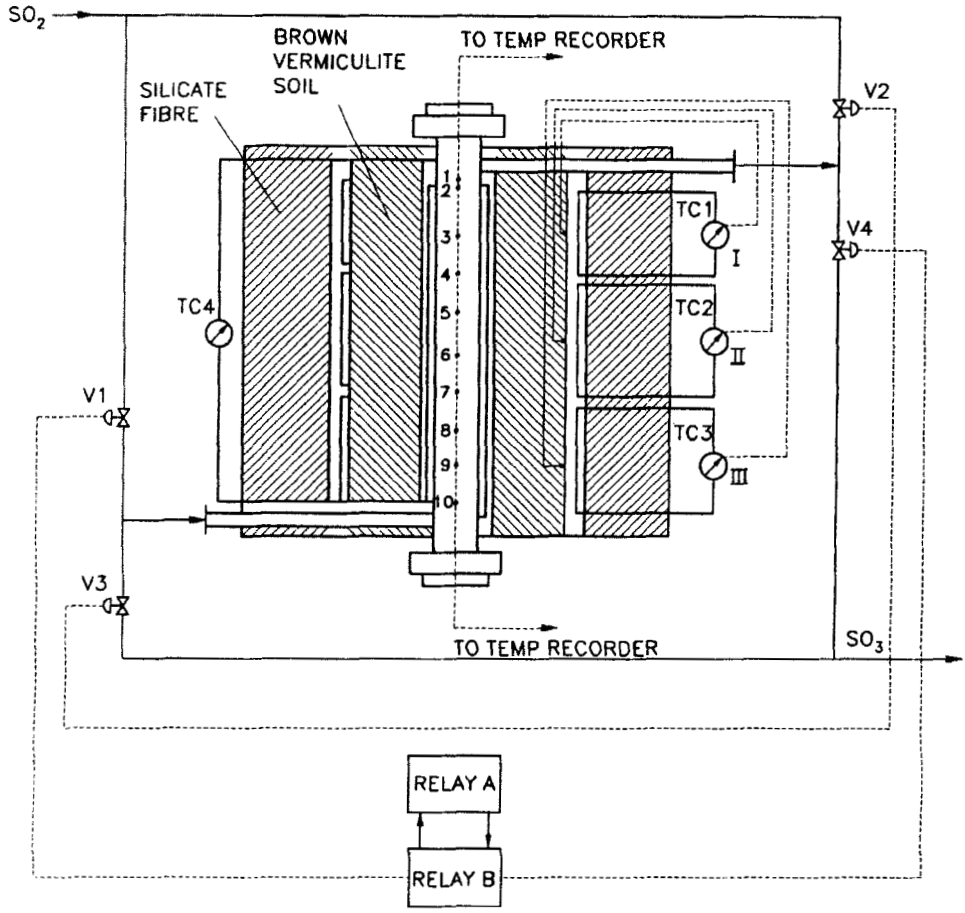

FIG. 11. Schematic of a research flow-reversal reactor showing switching valves and instrumentation. Heavy insulation was used to try to obtain adiabatic operation. (Figure adapted from Xiao and Yuan, 1996, with permission of the authors.)

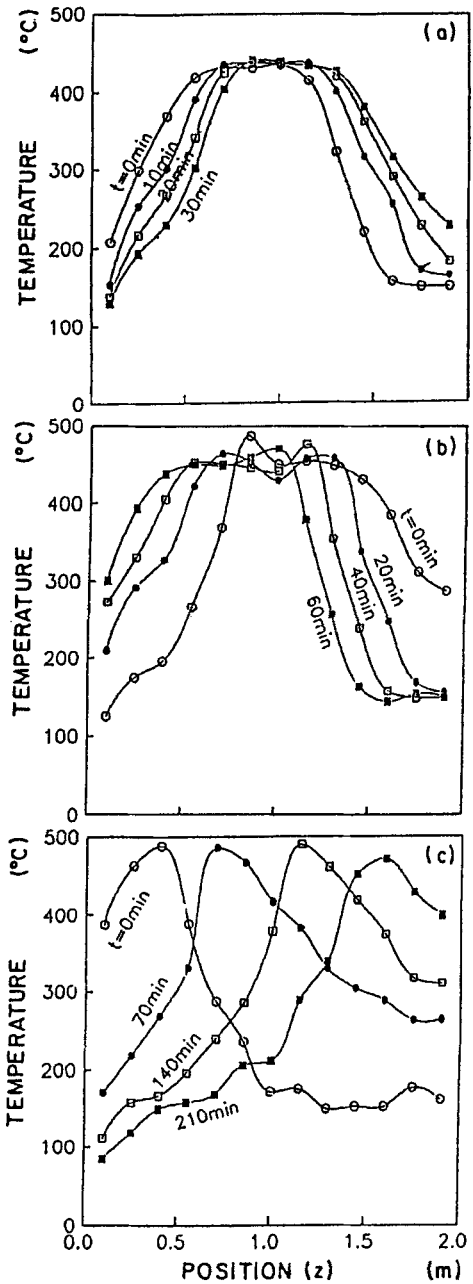

FIG. 12. Time change of temperature profiles in a catalyst bed under an invariant cycling state for an SO_2-containing feed entering the reactor at 25°C. Results for the Chinese S101 catalyst. (Figure adapted from Wu *et al.*, 1996, with permission of the authors.)

velocities, and cycle periods are given. In Fig. 12a, the curves for 0 and 30 min represent the start and end of a half cycle. A comparison of the (a) and (b) sections of the figure shows that increasing the throughput of reactant, just as for higher SO_2 levels in the feed and higher flow rates, raises the maximum temperature and extends the width of the high temperature zone. Figure 12a shows that about half of the bed is held at constant temperature. This temperature exceeds the adiabatic temperature rise for the feed by about 300°C. Movement of the temperature front through the bed can be seen in (c) of the figure. Increasing the cycle period above 420 min would have extinguished the reaction because the cold front, started at the time of switching by cold feed entering the bed, reaches the end of the bed.

C. Modeling and Simulation

If kinetic processes on catalytic surfaces in SO_2 oxidation are assumed to be at steady state, temperature and concentration fields in a radially symmetrical, adiabatic catalyst bed are described by the equations collected in Table IX for the reactor space $0 \leq z \leq L$ and time $t \geq 0$ (Matros, 1989; Matros and Bunimovich, 1996). The subscript p indicates a condition at the surface of a catalyst particle of radius R_p. A spherical particle has been assumed in Eq. (31). Rates are expressed in units of particle volume. Multiplying ρ_B converts them to mass units. Assuming plug flow through the reactor and neglecting radial temperature gradients reduces dimensionality. Matros (1989) contends that allowing for radial gradients in large-diameter, well-packed beds without wall anomalies has a negligible influence on front movement. Radial heat losses will be negligible if the reactor is insulated even when narrow beds are used.

Equations in Table IX are written per unit of bed volume; $(\lambda_l)_g$ is a time averaged, mean axial bed conductivity. D_l is a longitudinal diffusivity and λ_l allows for particle to particle conductivity. Not all the terms in the model as given in the table are important. For example, Wu *et al.* (1995, 1996) and Xiao and Yuan (1996) neglect the accumulation and dispersion terms in Eq. (30) and the accumulation and conduction terms in Eq. (28).

Because the term $r(C_A, T)$ is exponentially dependent on T and can be nonlinear as well, a numerical solution or piecewise linearization must be used. To simplify the numerical manipulations, equations in Table IX are normalized by $\xi = z/L$, $\tau' = ut/L$, and $x = 1 - C_i/(C_i)_o$, where i is normally SO_2. y also is a normalized quantity. The Péclet numbers for mass and heat are written $Pe_M = 2R_p u/D_l$ and $Pe_H = 2R_p c_p u/\lambda_l$ for a spherical particle. They are also written in terms of bed length as Bodenstein numbers. It is

TABLE IX

MODEL FOR A PACKED-BED CATALYTIC REACTOR WITH PERIODIC REVERSAL OF FLOW DIRECTION

Gas phase:

$$(\tilde{C}_p)_g \frac{\partial T}{\partial t} = + (\lambda_l)_g \frac{\partial^2 T}{\partial z^2} - (\tilde{C}_p)_g u \frac{\partial T}{\partial z} + h_p S_{ext}(T_p - T) \tag{28}$$

Solid phase:

$$(C_p)_p \frac{\partial T_p}{\partial t} = + \bar{\lambda}_l \frac{\partial^2 T_p}{\partial z^2} - h_p S_{ext}(T_p - T) + \frac{\Delta H_{ad} \bar{\eta}}{(1 - \varepsilon_B)} r(C_{A_{r=R_p}}, T_p) \tag{29}$$

Gas phase:

$$\varepsilon_B' \frac{\partial C_A}{\partial t} = D_l \frac{\partial^2 C_A}{\partial z^2} - u \frac{\partial C_A}{\partial z} - k_p S_{ext}(C_A - C_{A_{r=R_p}}) \tag{30}$$

Solid phase:

$$k_p(C_A - C_{A_{r=R_p}}) = \frac{R_p \bar{\eta}}{3} r(C_{A_{r=R_p}}, T_p) \tag{31}$$

Boundary conditions:

$$Z = 0 \qquad (-\bar{\lambda}_l)_f \frac{\partial T}{\partial z} = (c_p)_g u + (T - T^\circ) \tag{32}$$

$$\frac{\partial T_p}{\partial z} = 0 \tag{33}$$

$$-D_A \frac{\partial C_A}{\partial z} = u^+(C_A - C_A^\circ) \tag{34}$$

$$z = L, \qquad (-\bar{\lambda}_l)_g \frac{\partial T}{\partial z} = (C_p)_g u^-(T - T^\circ) \tag{35}$$

$$\frac{\partial T_p}{\partial z} = 0 \tag{36}$$

$$-D_A \frac{\partial C_A}{\partial z} = u^-(c_A - c_A^\circ) \tag{37}$$

$$t = t_o + \frac{n\tau}{2}, \quad n = 1, 2, 3 \ldots, \qquad T(z, t^-) = T(z, t^+) \tag{38}$$

$$T_p(z, t^-) = T_p(z, t^+) \tag{39}$$

$$C_A(z, t^-) = C_A(z, t^+) \tag{40}$$

where

$$u^+ = \max(u(t), 0), \qquad u^- = \max(-u(t), 0) \tag{41}$$

With flow from the left, u^+ will be positive and $u^- = 0$. When the flow is from right to left, $-u(t)$ is positive so $u^- = u(t)$, and $u^+ = 0$; t^-, t^+ designate instants before and after a flow direction switch.

TABLE X
SIMPLIFIED, DIMENSIONLESS FORM OF THE FLOW REVERSAL MODEL

$$C_r \frac{\partial \theta}{\partial \tau'} = \frac{1}{\text{Phs}} \frac{\partial^2 \theta}{\partial \xi^2} + \beta_1 r(\theta, y) - \alpha(\theta - T) \tag{42}$$

$$0 = \frac{1}{\text{Phg}} \frac{\partial^2 T}{\partial \xi^2} - \frac{\partial T}{\partial z} + \alpha(\theta - T) \tag{43}$$

$$\gamma(y - x) = \beta_2 r(\theta, y) \tag{44}$$

$$\frac{\partial x}{\partial \xi} = \beta_2 r(\theta, y) \tag{45}$$

with boundary conditions:

$$\xi = 0, \tau' > 0 \begin{cases} \dfrac{\partial \theta}{\partial \xi} = 0 \\ -\dfrac{1}{\text{Phg}} \dfrac{\partial T}{\partial \xi} + T = T_{\text{in}} \\ x = 0 \end{cases} \tag{46}$$

$$(\xi = 1, \tau' > 0) \begin{cases} \dfrac{\partial \theta}{\partial \xi} = 0 \\ \dfrac{\partial T}{\partial \xi} = 0 \end{cases} \tag{47}$$

$$\begin{aligned} \tau &= \frac{n}{2}\tau, \quad n = 1, 2, 3 \\ T(\xi, \tau^-) &= T(\xi, \tau^+) \\ \theta(\xi, \tau^-) &= \theta(\xi, \tau^+) \\ x(\xi, \tau^-) &= x(\xi, \tau^+) \\ y(\xi, \tau^-) &= y(\xi, \tau^+), \end{aligned} \tag{48}$$

this formulation that is used in Table X that gives the dimensionless form of the model (Xiao and Yuan, 1994).

Temperature and concentration differences between gas and catalyst can be neglected to give a pseudo-homogeneous model,

$$\frac{\partial X}{\partial \xi} + \kappa(1 - X) \exp\left(\frac{\theta}{B\theta + 1}\right) = 0 \tag{50}$$

$$\gamma \frac{\partial \theta}{\partial \tau'} = \frac{1}{(\text{Pe}_{\text{H}})} \frac{2R_p}{L} \frac{\partial^2 \theta}{\partial \xi^2} - \frac{\partial \theta}{\partial \xi} + \Delta\theta_{\text{ad}} \kappa(1 - X) \exp\left(\frac{\theta}{B\theta + 1}\right). \tag{51}$$

the higher order term allows for conductivity in the bed only.

TABLE X (*continued*)
SIMPLIFIED, DIMENSIONLESS FORM OF THE FLOW REVERSAL MODEL

where τ^- and τ^+ are the dimensionless times just prior to and after a direction switch.

$$\theta(z, 0) = \text{initial temperature profile} \tag{49}$$

$$\beta_1 = (1 - \varepsilon_B)\frac{(-\Delta H)}{(\rho C_P)_g T_0}\frac{L}{u}$$

$$\beta_2 = (1 - \varepsilon_B)\frac{L}{u}\frac{1}{C_{in}}$$

$$\alpha = (1 - \varepsilon_B)\frac{S_v h_P}{(\rho C_P)}\frac{L}{u}$$

$$\gamma = (1 - \varepsilon_B)S_v k_P \frac{L}{u}$$

$$C_r = (1 - \varepsilon_B)\frac{(\rho C_P)_s}{(\rho C_P)_g}$$

$$\frac{1}{\text{Phs}} = (1 - \varepsilon_B)\frac{(\lambda_l)}{(\rho C_P)_s u L}$$

$$\frac{1}{\text{Phg}} = \varepsilon_B \frac{(\lambda_l)_g}{(\rho C_P)_g u L}$$

$$\frac{1}{\text{Pmg}} = \varepsilon_B \frac{D_e}{uL}$$

Often in industrial-scale reactors, the lengths of reactors and gas velocities lead to large values of $\text{Pe}(L/2R_p)$ that make the contribution of the dispersion terms negligible. In this situation, the order of the set of PDEs is reduced and an accurate description of front movement can be made through piecewise linearization of the rate term and use of the elegant method of characteristics (Rhee and Amundson, 1974). Boreskov *et al.* (1977) note that the pseudo-homogeneous model gives an adequate approximation for flow reversal. Eigenberger and Nieken (1988) also used this packed-bed model in their study of flow reversal.

The ultimate simplification is

$$\frac{(\lambda_l)_g}{(c_p)_g u L}\frac{d\theta}{d\xi} = \frac{1}{2}\Delta T_{ad}(X_1 - X_2) \tag{52}$$

$$\nu_{sv}\frac{dX_1}{d\xi} = \frac{1}{2}r(\theta, X_1) \tag{53}$$

$$\nu_{sv}\frac{dX_2}{d\xi} = \frac{1}{2}r(\theta, X_2). \tag{54}$$

The boundary conditions are

$$\xi = 0: \quad X_2 = X_f, \qquad \theta = T^o + \Delta T_{ad} X_f \tag{55}$$

$$X_1 = 0$$

$$\xi = 1: \quad X_1 = X_2. \tag{56}$$

In these equations, $\xi = 0$ is the bottom of the catalyst bed and X_1 is the conversion in the flow direction from bottom to top, while X_2 is the conversion in the opposite flow direction. Bunimovich *et al.* (1990) suggest using Eqs. (52) to (54) for an initial estimate of the temperature profiles in order to speed up conversion on integration of the full model equations in Table X. This step would only be taken if it were the stationary cyclic state profiles that are wanted.

A substantial literature, mainly in Russian, discusses the simulation of various industrial processes operating under flow reversal. Much of this work deals with SO_2 oxidation. For the rate term, Russian researchers (Boreskov *et al.*, 1982) used the expression

$$r_{SO_2} = k \frac{P_{SO_2} - (P_{O_2})^{1/2}(1 - \beta)}{(1 + K_{ad}(P_{SO_3})^{1/2})}. \tag{57}$$

The β term allows for the reverse reaction, and it is usually written

$$\beta = \frac{P_{SO_3}}{K P_{SO_2}(P_{O_2})^{1/2}}. \tag{58}$$

The rate model contains four adjustable parameters, as the rate constant k and a term in the denominator, K_{ad}, are written using the Arrhenius expression and so require a preexponential term and an activation energy. The equilibrium constant can be calculated from thermodynamic data. The constants depend on the catalyst employed, but some, such as the activation energy, are about the same for many commercial catalysts. Equation (57) is a steady-state model: the low velocity of temperature fronts moving through catalyst beds often justifies its use for periodic flow reversal.

The calculated conversions presented in Table VIII used Eq. (57). They are quite remarkable. They reproduce experimental trends of lower conversion and higher peak bed temperature as the SO_2 content in the feed increases. Bunimovich *et al.* (1995) compared simulated and experimental conversion and peak bed temperature data for full-scale commercial plants and large-scale pilot plants using the model given in Table IX and the steady-state kinetic model [Eq. (57)]. Although the time-average plant performance was predicted closely, limiting cycle period predicted by the

model are much longer than experimental limits. Periods used in plant operation were between 25 and 60% of this limit.

There are many other SO_2 simulation using the models described in Tables IX and X or their further simplifications (Boreskov and Matros, 1984; Matros, 1989; Bunimovich *et al.*, 1990; Sapundzhiev *et al.*, 1990; Snyder and Subramanian, 1993; Xiao and Yuan, 1994, 1996; Zhang *et al.*; 1995; Wu *et al.*, 1996). These simulations are capable of reproducing operating data as demonstrated in Table VIII and in the preceding discussion. They have been useful in understanding the application of periodic flow reversal to SO_2 oxidation, as we shall see.

A simplified version of the model in Table IX, neglecting accumulation of mass and heat as well as dispersion and conduction in the gas phase, predicts dynamic performance of a laboratory SO_2 converter operating under periodic reversal of flow direction quite well. This is shown by Fig. 13 taken from Wu *et al.* (1996). Data show the temperature profiles in a 2-m bed of the Chinese S101 catalyst once a stationary cycling state is attained. One set of curves shows the temperature distribution just after switching direction and the second shows the distribution after a further 60 min. Simulated and experimental profiles are close. The surprising result is that the experimental maximum temperatures equal or exceed the simu-

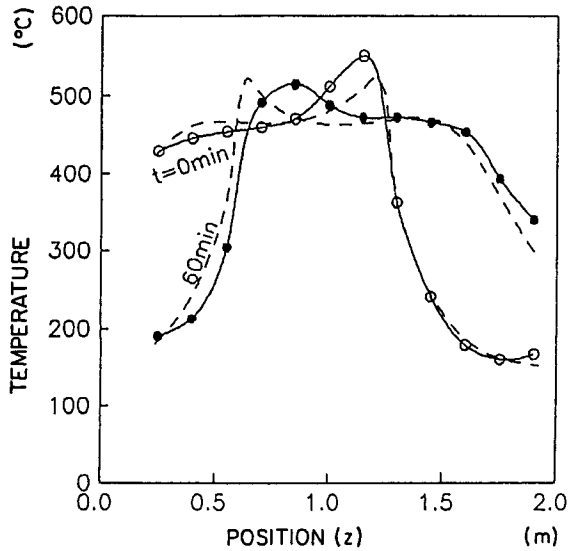

FIG. 13. Comparison of simulated and experimental temperature profiles in a 2-m, near-adiabatic, packed-bed SO_2 reactor using a Chinese S101 catalyst and operating under periodic reversal of flow direction with τ = 180 min, SV = 477 h^{-1}, and inlet SO_2 = 3.89 vol% and T = 25°C. (Figure adapted from Wu *et al.*, 1996, with permission of the authors.)

lated values. The model is adiabatic, but the reactor cannot be operated without heat loss, so experimental values should fall below the simulated results. In an earlier paper employing the same model, Zhang *et al.* (1995) explored the effect of catalyst bed length, L, inlet SO_2 concentration, space velocity, and cycle period τ on SO_2 conversion and the peak bed temperature. With respect to concentration and space velocity, simulation results agreed with Russian work and experimental data shown in Table VIII: Increasing SO_2 vol% and SV decrease conversion, but increase the peak bed temperature. Bed length has the opposite effect: Conversion increases and peak temperature decreases as the depth of the catalyst bed is augmented. Increasing τ increases both conversion and peak temperature, but the change is small over a 3 $\times$ change of cycle period. Both Zhang *et al.* (1995) and Wu *et al.* use a version of the rate expression given by Eq. (57) in their simulations.

Xiao and Yuan (1994, 1996) used a model similar to that given in Table X for a comprehensive investigation of SO_2 oxidation in an adiabatic packed bed employing flow reversal. Figure 14 illustrates the effect of inlet SO_2 concentration on reactor operation during periodic switching of the flow direction. Figure 14a nicely shows the increase in maximum bed temperature and in width of a zone of high, near-constant temperature as the inlet vol% SO_2 rises. Figure 14b gives the effect of inlet concentration on maximum temperature, SO_2 conversion, and the velocity of the moving temperature fronts. The figure shows that there is a minimum inlet concentration of about 1.2 vol% for a stable reaction. This minimum depends on O_2 concentration, inlet temperature, catalyst, and space velocity. Increasing space velocity reduces the minimum. The reason for its existence, shrinking of the zone of high and near-constant temperature, can be seen in Fig. 14a. Above the minimum inlet concentration, the peak bed temperature increases rapidly with rising SO_2 concentration in the feed. The temperature extends from 400°C because this was the startup temperature. It is often convenient to express the concentration effect in terms of the adiabatic temperature rise, ΔT_{ad}. This approach is favored by Russian investigators (Matros, 1989). Returning to Fig. 14b and noting that the SO_2 concentration is proportional to ΔT_{ad}, then once the minimum ΔT_{ad} is reached, the reaction is stabilized. Increasing ΔT_{ad} only increases the maximum temperature in the catalyst bed. This increase is about the same as the increase in ΔT_{ad}. Increasing temperature causes a maximum in SO_2 conversion that is shown in the plot. This reflects the importance of the reverse reaction at high temperatures. Finally, Fig. 14b shows that the variation of velocity of the temperature front with the inlet SO_2 vol% is small. All these results are for $\tau = 30$ min and SV = 514 h^{-1}.

Xiao and Yuan (1996) also explored the effect of replacing the front

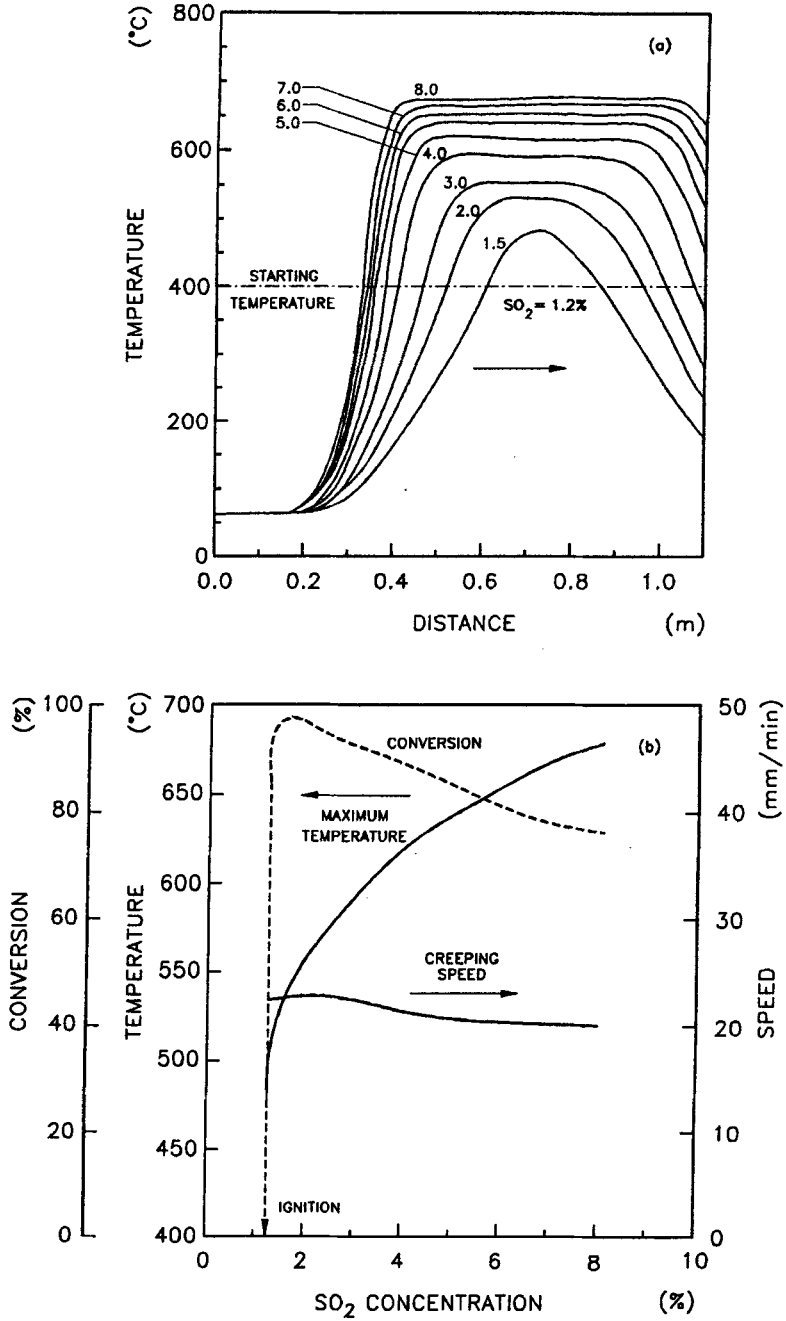

FIG. 14. Influence of inlet SO_2 concentration on behavior and performance in adiabatic, packed-bed SO_2 converters operating under periodic flow reversal. Simulation results for τ = 30 min, SV = 514 h^{-1}, T_o = 25°C: (a) effect of inlet SO_2 vol% on the temperature profile in the catalyst bed, (b) influence of inlet SO_2 on converter performance and the velocity of the temperature front. (Figure adapted from Xiao and Yuan, 1996, with permission of the authors.)

and back portions of the bed by an inert packing as depicted in Fig. 7. This packing functions as a heat recuperator. The simulation of Xiao and Yuan demonstrates that these zones are below the temperature required for the reaction to proceed for most of a cycle so that catalyst in these zones is nonfunctional. Furthermore, these zones experience temperature fluctuations reaching up to 300°C when there is a flow direction switch. The inert zones augment the temperature of the gas entering the catalyst bed and thereby increase temperatures in the bed. This reduces conversion. There is a strong time-in-cycle effect caused by inert packing as shown in Fig. 15. Higher temperature at the end of the catalyst section as the half cycle progresses decreases SO_2 conversion through the reverse reaction, causing the drop shown in the figure for 0.2 m of noncatalytic packing on each end of the catalyst bed. The simulation assumes tau; = 30 min and SV = 514 h^{-1}. The inlet SO_2 concentration is 2.62 vol%. Matros (1989) observed the effect of recuperator zones earlier. He also noted that the presence of these zones extends the maximum cycle period before blowout of the reaction occurs.

Xiao and Yuan (1994) also studied startup, and a large wrong-way behav-

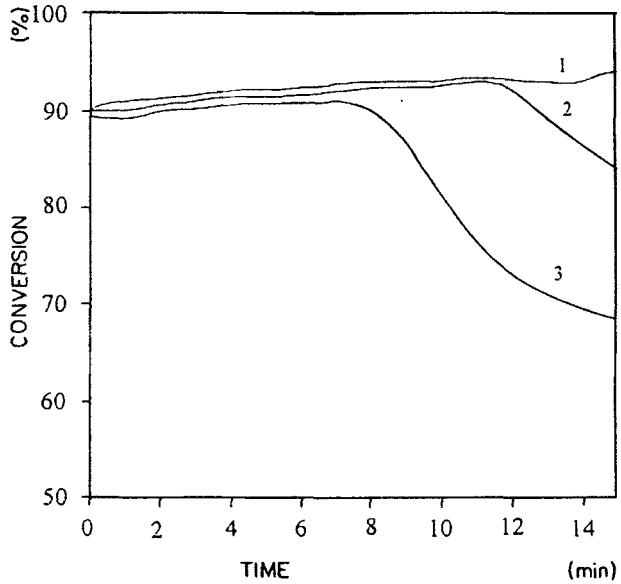

FIG. 15. Variation of SO_2 conversion with time within a half cycle based on simulation of the reactor in Fig. 14 and for the conditions given in that figure with inlet SO_2 = 2.62 vol%. Curve 1, full 1.4-m bed filled with catalyst; curve 2, 0.1-m regions filled with noncatalytic packing at both ends of the catalyst bed; curve 3, 0.2-m regions instead of 0.1-m ones. (Figure adapted from Xiao and Yuan, 1996, with permission of the authors.)

ior was seen when cold feed is introduced. A sharp temperature jump occurs near the entrance to the bed that could be large enough to damage catalyst. The magnitude of the temperature jump depends strongly on the SO_2 concentration as well as other operating conditions. Xiao and Yuan successfully simulated the dynamic operation of their laboratory reactor and comment that the match between model and data can be improved by allowing for radial heat loss in their model. This was accomplished by adding a heat transfer term to Eq. (28) in Table IX. The reactor model remains one-dimensional.

Bunimovich *et al.* (1984) point out that if the period of flow reversal, τ, is very small relative to the time required for the temperature front to creep through the bed and the high-temperature zone occupies most of the bed; a relaxed steady state is achieved in which the temperature profile is constant through most of the bed. This profile can be calculated and leads to a steady-state model for this extreme variant of flow reversal.

Both Matros (1989) and Eigenberger and Nieken (1988) mention potential operating problems identified using the model summarized in Table IX. For any operation there is a minimum feed temperature for ignition. At temperatures above this minimum, a stable temperature profile is achieved after several reversal cycles. Flow reversal can tolerate lower concentrations and even the absence of reactants for time periods $\Delta t < \tau$. Concentration increases, for exothermic reactions, lead to abrupt increases in the maximum bed temperature that may cause catalyst deactivation or even damage to the reactor vessel. The problem of high reactant concentrations has inspired a number of multibed flow-reversal schemes that are discussed by Matros (1989). When process upsets upstream of the flow-reversal reactor cause reactant concentration excursions; control can be handled by recycle to dilute the stream, by diverting reactant flow at points within the reactor, or by adding thermal ballast in the form of a boiler or a liquid-phase heat exchanger. Purwono *et al.* (1994) have examined the last suggestion experimentally and through simulation. A theoretical lower limit on cycle period exists (Van den Bussche *et al.*, 1993) and there is an upper limit discussed when experimental results were considered. This period is predictable. There is also a maximum period at startup in order to ignite the reaction. Eigenberger and Nieken (1988) found that these maximum periods are not the same.

A concern in the application of periodic flow reversal to converting SO_2 in smelter emissions is the variability of these emissions. Both SO_2 concentration and gas volume may vary, often irregularly. Like startup, this is a matter that could profit from simulation studies using models discussed in this section.

Bunimovich *et al.* (1995) have applied the Balzhinimaev model for SO_2

oxidation over vanadia catalysts to a nonisothermal tubular reactor with periodic flow reversal. The model is probably too complicated for wide use, as it appears from the preceding discussion that steady-state models give adequate results for most simulation studies. These earlier models assume that the steady-state kinetics apply under the slowly changing conditions of periodic flow reversal, but they overpredict the time average SO_2 conversions by about 1% at low inlet SO_2 levels. They also fail to predict an experimentally observed low level in the SO_3 content of the effluent after switching followed by a slow rise until the concentration slightly exceeds the SO_2 concentration in the converter feed. After this maximum, SO_3 sinks slowly until it falls below the inlet SO_2 level. (Steady-state models do not show this, as may be seen in Fig. 15.) Allowing for the dynamics of the catalyst using the kinetic model given in Table IV, Bunimovich *et al.* (1995) demonstrate that predicted conversions fall below those given by the steady-state kinetic model thereby realizing better agreement with experimental data. They also show that dissolution of SO_3 from the melt is slow, and it is this that accounts for the initial low level of SO_3 in the effluent and its subsequent rise and overshoot. Improved dynamic prediction that the unsteady-state kinetic model of Balzhinimaev offers is important for the design of control systems for flow reversal, but is not necessary for exploring applications of periodic flow reversal to acid plant or smelter effluents where only the time-average performance is of interest.

Bunimovich *et al.* (1995) lumped the melt and solid phases of the catalyst but still distinguished between this lumped solid phase and the gas. Accumulation of mass and heat in the gas were neglected as were dispersion and conduction in the catalyst bed. This results in the model given in Table V with the radial heat transfer, conduction, and gas phase heat accumulation terms removed. The boundary conditions are different and become identical to those given in Table IX, expanded to provide for inversion of the melt concentrations when the flow direction switches. A dimensionless form of the model is given in Table XI. Parameters used in the model will be found in Bunimovich's paper.

It is instructive to examine predictions of the Bunimovich *et al.* model. The temperature profiles in Fig. 16a at times within a half cycle are about the same as the profiles for 6 vol% SO_2 predicted by Xiao and Yuan (1996) and shown in Fig. 14a. Note that curves 1 and 5 in Fig. 16 are those at the switching time and show the inversion when the flow direction changes. The remarkable prediction of the Table XI model is the sharp variation of the SO_3 concentration in the melt with position in the bed that develops about 1 min after the direction changes and persists for about 13 min. Curves (c) to (f) show there is a substantial change in the complexes present in the melt with position in the bed and that the complex concentrations

TABLE XI

PERIODIC FLOW REVERSAL MODEL EMPLOYING THE BALZHINIMAEV UNSTEADY STATE KINETIC MODEL FOR SO_2 OXIDATION OVER VANADIA CATALYSTS (BUNIMOVICH *ET AL.*, 1995)

$$\gamma_\theta \frac{\partial \Theta}{\partial \tau} = \gamma_D \Delta T_D \frac{\partial C_3^L}{\partial \tau} + \Lambda \sum_{i=1}^{4} \Delta T_i r_i - \alpha(\Theta - T) \tag{59}$$

$$\gamma_D \frac{\partial C_3^L}{\partial \tau} = \beta_3 \left[x_3^f - \frac{C_3^L}{H_3 P(1 - C_3^L/C_o)} \right] + \Lambda \sum_{i=1}^{4} \nu_{3i} r_i \tag{60}$$

$$\gamma_\theta \frac{\partial \theta_m}{\partial t} = \sum_{i=4}^{4} \mu_i r_i, \qquad m = \overline{1,3} \tag{61}$$

$$\frac{\partial x_j^f}{\partial \xi} = \beta_j (x_j^f - x_j), \qquad j = \overline{1,3} \tag{62}$$

$$\frac{\partial T}{\partial \xi} = \alpha(\Theta - T) \tag{63}$$

$$\Lambda \sum_{i=1}^{4} \nu_{ji} r_i = \beta \left(x_j^f - \frac{C_j}{H_j P} \right), j = 1, 2, \tag{64}$$

with boundary and initial conditions

At $\xi = 0$:

$$T = T_{in}, \qquad x_j^f = (x_j^f)_{in}.$$

At $\tau = 0$:

$$\Theta = \Theta_0(\xi); x_3^L = (x_3^L)_0(\xi); \quad \theta_m = (\theta_{m,0})(\xi) \tag{65}$$

$$(m = \overline{1,3})$$

$$\tau = t_c, \frac{n\tau}{2}, n\tau^* \qquad n = 1, 2, 3, \ldots$$

$$\begin{aligned} \theta_m(\xi) &= \theta_m(1 - \xi), \quad x_j^f(\xi) = x_j^f(1 - \xi) \\ C_3^L(\xi) &= C_3^L(1 - \xi), \Theta(\xi) = \Theta(1 - \xi) \\ T(\xi) &= T(1 - \xi) \end{aligned} \tag{66}$$

can be described in terms of sharply defined moving fronts. V^{4+} represents the concentration of catalytically inactive vanadium. Relatively high levels shown in Fig. 16f reflect low temperatures in the front of the bed and the high level of SO_3 in the outlet. Both conditions cause vanadium reduction. The SO_2 and O_2 curves in Figs. 16g and 16h show a concentration front moving through the bed with a narrow reaction zone. The SO_3 profile is unusual: Just after the switch SO_3 leaving the catalyst bed drops to zero.

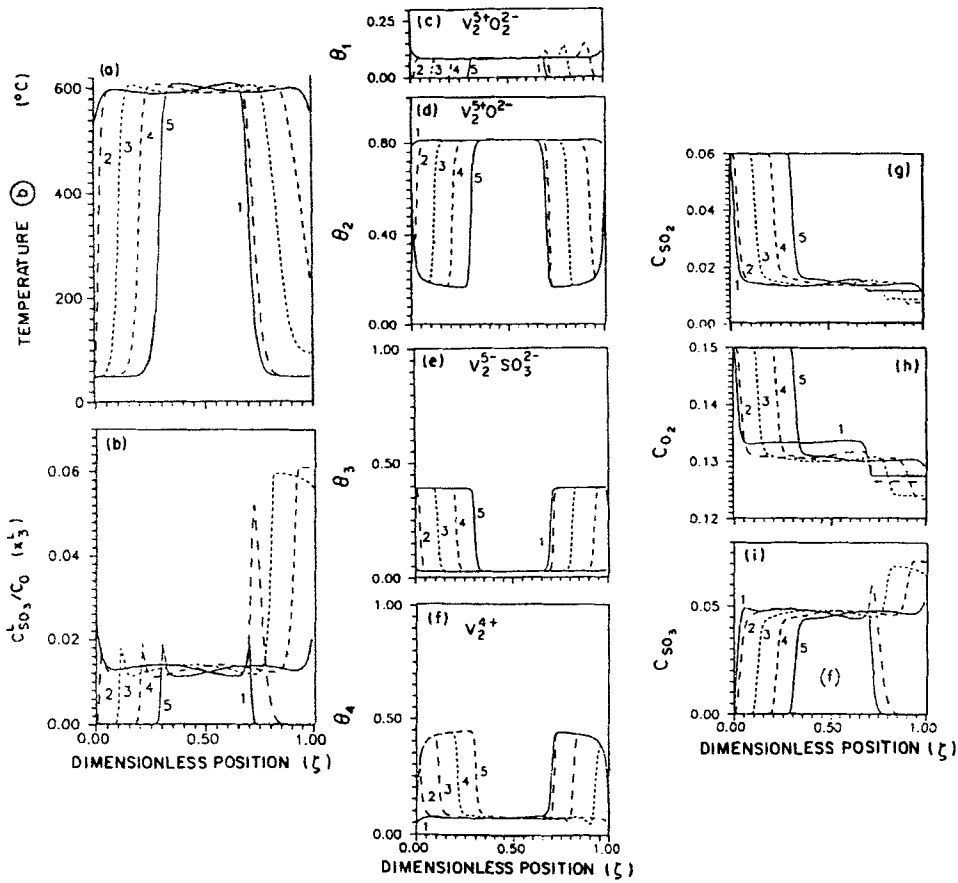

FIG. 16. Variation in a stationary cycling state of catalyst temperature, SO_3, and complex concentrations in the melt phase and the concentration of gas phase species with time in a half cycle in the forward flow portion of a reactor operating under periodic reversal of flow direction with τ = 40 min, SV = 900 h^{-1}, $(C_{SO2})_o$ = 6 vol%, $(C_{O2})_o$ = 15 vol%, T_o = 50°C. Curves: 1, just after switching flow direction; 2, 1 min; 3, 6.6 min; 4, 13.3 min, and 5, 20 min after a switch in flow direction. (Figure adapted from Bunimovich *et al.*, 1995, with permission, © 1995 Elsevier Science Ltd.)

By 6 min into the half cycle, buildup of the SO_3 concentration in the melt (see Fig. 16b) and decreasing SO_3 solubility with rising temperature results in a significant rise in SO_3 leaving the catalyst bed. This continues for some 13 to 14 min into the half cycle and then drops.

Model dynamics were forced to steady state by setting derivatives for the melt complexes in Eq. (61) to zero (Bunimovich *et al.*, 1995). This should make the model behave as though the steady-state kinetic model

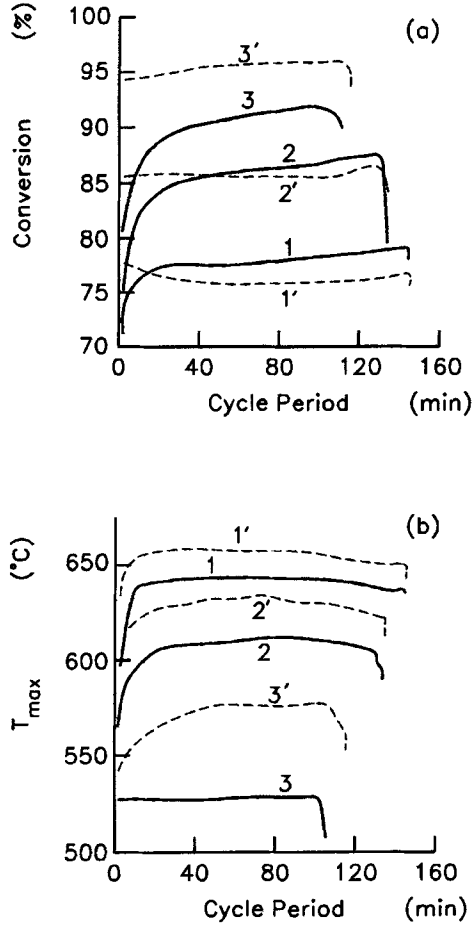

FIG. 17. Comparison of the variation of the time-average SO_2 conversion and the maximum bed temperature predicted for stationary cycling condition by an unsteady-state and a steady-state kinetic model for a packed-bed SO_2 converter operating with periodic flow reversal under the input conditions given in Fig. 16: unsteady-state model—, steady state model-------. Curves: 1,1', $(C_{SO2})_o$ = 9 vol%; 2,2', $(C_{SO2})_o$ = 6 vol%; 3,3', $(C_{SO2})_o$ = 3 vol%. (Figure adapted from Bunimovich *et al.*, 1995, with permission, © 1995 Elsevier Science Ltd.)

were in use, except for SO_3 solubility variations as temperature changes. Figure 17 compares SO_2 conversion and the peak bed temperatures for the dynamic kinetic model with those for its steady-state version. With relatively high inlet SO_2 levels, 9 vol%, conversion predictions differ by about 3% with the dynamic model providing higher conversions. Temperatures are only 10 to 15°C apart. With 6 vol% SO_2 in the feed, both unsteady-

state and steady-state kinetic models predict the same conversions. Maximum temperature prediction differences increase to about 20°C. When $(C_{SO2})_o$ = 3 vol%, conversions predicted by the steady-state kinetic model were about 5% greater than those predicted by the unsteady-state model. Differences in the predicted maximum temperatures grew to 40°C. Bunimovich *et al.* point out that the simulation using the steady-state kinetic model gave poorer predictions of the experimental data in Table VIII when the inlet SO_2 level dropped under 3 vol%.

D. Overview

Simulation as well as experimental measurements demonstrate features of periodic flow reversal that account for its successful application to SO_2 oxidation: (1) a region of uniform high temperature in the reactor center that is essentially time invariant, (2) a profile consisting of a maximum temperature followed by diminishing temperature in the flow direction, which results in higher conversions for equilibrium-limited, exothermic reactions, (3) overall conversion or outlet concentrations that show little variation with time, and (4) outlet temperatures close to inlet temperatures. Reactors employing periodic reversal of flow direction offer lower capital cost because heat recovery is performed by the catalyst bed or by a packed-bed recuperator instead of a shell and tube heat exchanger. Reactors using flow reversal appear to be able to handle small variations of operating conditions without resorting to process control because of the large thermal inertia they provide. For exothermic, equilibrium-limited reactions, such as SO_2 oxidation, the declining temperature profile toward the end of the reactor is probably the primary advantage offered.

IV. Conversion of SO_2 in Trickle-Bed Catalytic Scrubbers Using Periodic Flow Interruption

Periodic operation of three-phase reactors is a new area of study. Mass transfer of gaseous reactants through the liquid phase limits many trickle-bed processes. One way of increasing the rate of mass transfer and thereby rates in three-phase reactors is to segregate the gas and liquid phases using structured packing formed from a catalytically active, porous membrane. This arrangement provides access to the catalyst surface without transport through the liquid phase. Yang and Cussler (1987) discuss such a system.

Plate type packing to separate the phases is discussed by Carlsson *et al.* (1983) and by Hatziantoniu *et al.* (1986). De Vos *et al.* (1982, 1986) describe use of a monolithic porous catalyst with vertical and horizontal channels. The liquid phase flows downward through an array of parallel channels in the monolith, while gas moves in cross flow through a separate set of channels. Another approach treats the catalyst to make part of the surface hydrophobic or lyophobic (Berruti *et al.,* 1984). The gas phase has direct access to the surface on these unwetted portions of the surface, resulting in partial, spatial segregation of the phases.

Periodic flow interruption can be thought of as a type of partial segregation. It is a temporal segregation rather than a spatial one. The converse of periodic flow interruption is periodic flooding. Hot spots are observed in industrial-scale trickle beds and are thought to occur because of nonuniform irrigation of the catalyst by the liquid phase, often a consequence of low liquid loading. Periodic flooding fully irrigates the bed and is thus a means of avoiding hot spots. To carry this concept further, a low irrigation rate causes local temperatures to rise. If the liquid is near its boiling point, evaporation can take place. This removes the liquid phase from the catalyst surface and allows direct access for the gas phase. In situations where mass transfer through the liquid is limiting, direct access raises the temperature and thereby the rate of reaction substantially. Once the liquid phase evaporates completely, the rate of reaction diminishes and the location cools. It can then be reflooded by the liquid phase. This process can be replicated for an entire trickle bed by stopping and restarting liquid flow through the bed. Interrupting liquid flow in this way causes a temporary increase in the temperature of the catalyst bed, and thus higher rates and perhaps a selectivity improvement if higher temperatures favor better selectivity. It can also lead to catalyst overheating and runaway if the duration of the flow interruption is too long. Choice of cycle period and cycle split, however, control the duration and thus the temperature rise.

For their experimental investigation of flow interruption, Haure *et al.* (1989) chose the catalytic oxidation of SO_2 over a high-surface-area activated carbon catalyst. Several research groups have studied this catalytic reaction and kinetics are available. It proceeds rapidly at 25°C and is controlled, at least partially, by O_2 transport through the liquid phase.

A. Experimental Studies

A 40-mm i.d. Lucite column served as the reactor for the experiments of Haure *et al.* (1989). Reactor and feed system are shown schematically

in Fig. 18. Attention was paid to the distribution of the liquid phase: liquid was introduced onto the top of an array of parallel tubes that distributed the phase uniformly over a packing of fine glass helices. The helices were in direct contact with the 14/30-mesh, BPL activated carbon, a coal based material, produced by the Calgon Carbon Corp. Bed depth was kept constant at 160 mm in all experiments. Thermocouples were located at 30, 80, and 140 mm below the top of the carbon bed, but the points just penetrated the Lucite walls and did not extend into the bed. Water, the liquid phase, was saturated with air prior to entering the reactor. An overflow tank and system of two-way solenoid valves, in parallel, and a needle valve provided flow interruption and precise flow control. The gas, made up of 1.3 vol% anhydrous SO_2 and 98.7 vol% dry air, flowed continuously through the reactor at a rate of 25.4 ml (STP)/s. This corresponds to a space velocity of 800 h^{-1}.

In Haure's work, the gas phase leaving the reactor was not analyzed.

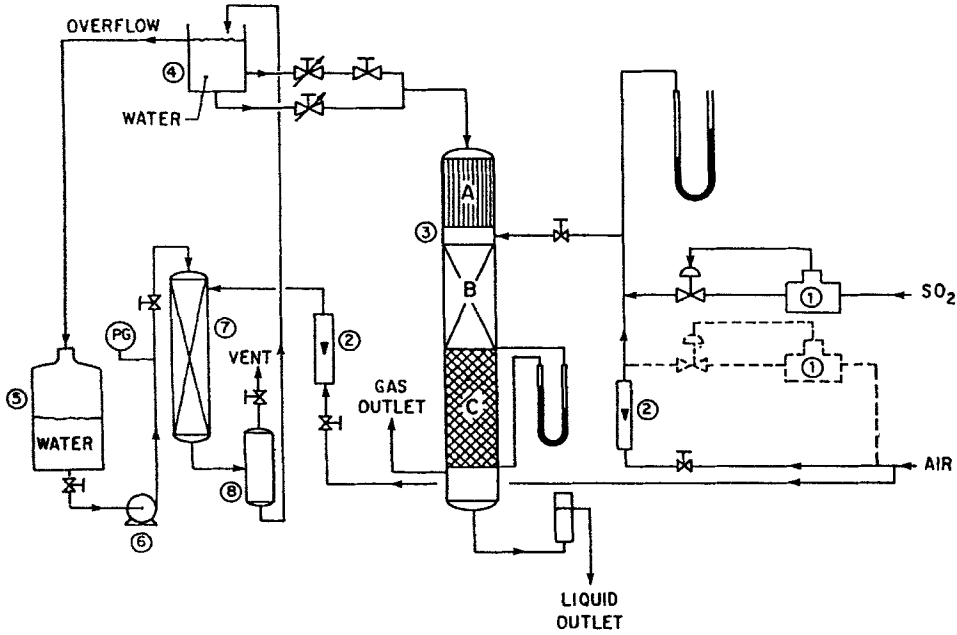

FIG. 18. Experimental trickle-bed system: A, tube bundle for liquid flow distribution; B, flow distribution packing of glass helices; C, activated carbon trickle bed; 1, mass flow controllers; 2, gas or liquid rotameters, 3, reactor (indicating point of gas phase introduction); 4, overflow tank for the liquid phase feed; 5, liquid phase hold-up tank; 6, absorber pump; 7, packed absorption column for saturation of the liquid phase; 8, gas–liquid disengager in the liquid phase saturation circuit. (Figure from Haure *et al.*, 1989, with permission, © 1989 American Institute of Chemical Engineers.)

Conversion and the mean rate of reaction were obtained by titrating the liquid recovered from the bed for total acidity before and after dissolved SO_2 and sulfurous acid were oxidized to sulfuric acid. The difference between these measurements allowed calculation of the SO_2 conversion. An extension of the Haure study (Metzinger *et al.*, 1992) added gas phase analysis and a check of the results through a sulfur balance. Computer control of flow interruption and acquisition of the SO_2 analyzer readings were also added.

Haure *et al.* (1989) conducted an exploratory investigation that considered the effect of cycle period, τ, cycle split, s, and time-average liquid superficial velocity, SV, on the spatial and time-average rate of oxidation. Cycle split, in this case, is the fraction of a period in which the liquid phase flows through the trickle bed. Figure 19 shows how these cycling variables affect the rate. Note that the period scale is logarithmic and data cover a range from 1 to 120 min. The figure also compares performance under periodic flow interruption with operation under steady state. The latter is given in the figure for the time-average liquid flow rate as the horizontal band in the center of the figure. These steady-state rates decrease as the time-average flow rate increases. The maximum steady state rate occurs

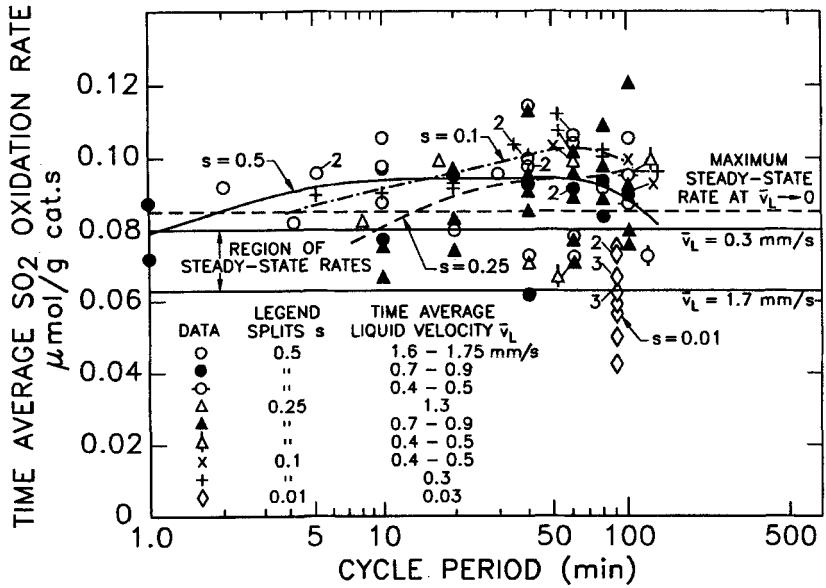

FIG. 19. Time-average rate of SO_2 oxidation under periodic liquid flow interruption as a function of cycle period, cycle split, and the time-average superficial liquid velocity at 26°C, 1 bar using a BPL activated carbon. (Figure from Haure *et al.*, 1990, with permission, © 1990 Elsevier Science Publishers.)

when the bed is loaded with liquid, but the phase is not flowing. The dashed horizontal line for a zero time-average liquid flow rate indicates this condition. Most of Haure's experimental data fall above the steady-state band and the maximum rate line. There is a separate symbol for each s and time-average liquid flow rate. The number beside a symbol indicates the number of data points the symbol represents. Curves shown in the figure have been drawn through data sets at $s = 0.5, 0.25$, and 0.1, neglecting the variations of the time-average liquid flow rates.

An exception to improved performance under flow interruption is for a group of points at $\tau = 90$ min with $s = 0.01$. In these experiments water flowed through the trickle bed for less than 1 min during a cycle. The oxidation rate under steady state is close to the maximum steady-state rate. Even though the scatter of the experimental data at $s = 0.01$ is large, all the measurements under flow interruption lie below the line representing steady state.

The flow interruption data shown in the figure suggests that at any cycle split, s, there is a minimum cycle period needed for the time-average rate of SO_2 oxidation to exceed the maximum rate under steady-state operation. Once above this period, increasing τ exerts just a small effect on the rate until τ reaches about 120 min, when rate may begin to drop. The experimental data are inadequate to indicate an optimal period accurately. The cycle split, s, clearly affects the time-average oxidation rate. Notwithstanding the curves for different values of s shown in Fig. 19, the data do not indicate an optimal s. The time-average liquid flow rate also influences the time-average rate under flow interruption, and the data reflected in each of the three s curves in the figure cover a different range of time-average liquid flow rates. As may be seen from the caption in the figure, measurements made at $s = 0.1$ employed time-average liquid phase velocities between 0.3 and 0.5 mm/s, whereas those at $s = 0.5$ used velocities between 0.4 and 1.75 mm/s. Replotting the $s = 0.5$ data showed that at 1.65 mm/s the rate improvement is between 40 and 65%. At a time-average liquid velocity of 0.86 mm/s, the rate improvement drops to about 20%.

Haure *et al.* (1989) also undertook experiments in which the liquid flow rate was periodically reduced rather than interrupted. Switching between time-average liquid velocities of 4.0 and 1.2 mm/s at $s = 0.5$ resulted in about a 10% increase in the time-average rate of SO_2 oxidation over steady state. The rate improvement was independent of τ over the 2 to 60 min range explored. This is considerably less than the increase when flow interruption is utilized.

Part of the explanation for increased rates under flow interruption rests

on the concept of segregation introduced earlier. At low liquid loading of a trickle bed, the external surface of a catalyst pellet is incompletely wetted. There is then direct access of the gas-phase reactants to the catalyst surface and, since both reactants are in the gas phase, higher oxidation rates are observed. Substantiation comes from steady-state measurements (Haure *et al.,* 1992) that show a rise in SO_2 oxidation rate as the superficial liquid velocity, u, drops below 2 mm/s. This results from a decrease in wetting of the carbon catalyst as the liquid loading is reduced. There is also a rise in rate with increasing velocity above $u = 4$ mm/s caused by growing liquid-phase turbulence that augments the liquid-phase volumetric mass transfer coefficient. A consequence of these divergent trends is a minimum when the oxidation rate is plotted vs the liquid velocity. A minimum has been observed by others for aqueous trickle-bed systems (Ramachandran and Smith, 1979; Tan and Smith, 1980; Mata and Smith, 1981) and also for nonaqueous systems (Sedricks and Kenney, 1973; Satterfield and Ozel, 1973), so it appears to be a general phenomenon.

Periodic flow interruption changes liquid loading on a trickle bed from moderate or high to zero. Even at zero loading, the carbon bed is partially wetted through static hold-up. Because of the continued presence of water, oxidation proceeds at a high rate. If a low split is used, the bed operates for most of the cycle at the high oxidation rate. Indeed, performance under flow interruption or reduction can be predicted as illustrated in Fig. 20. The curve in this schematic shows the steady-state data mentioned above extrapolated to $u = 0$. The two operating states are SS_1 and ASS_2; the "A" signifies it is an apparent operating state because if the trickle bed is held at zero liquid loading for a long enough time, the liquid holdup eventually evaporates and the rate decays to zero as SO_3 poisons the catalyst surface. The zero rate condition, SS_2, is the extreme of other possible operating states, which must lie below ASS_2. A surprising result of the Haure study is that the trickle bed functions at the ASS_2 state for up to 120 min after liquid flow has been halted. Consequently, neglecting any dynamic behavior, the time-average rate of reaction will be the steady-state rate at the two states weighted by the relative duration the bed remains in each of the states. The latter depends on the cycle split. In Fig. 20, $s = 0.5$ and the virtual operating state (VSS in the schematic) is midway on the straight line joining ASS_2 and SS_1. The rate at VSS is clearly considerably higher than the steady-state rate at a time-average superficial liquid velocity (CSS in the figure). The figure also shows the oxidation rate at the quasi-steady-state operating point (QSS). This is a point on a straight line joining SS_1 and SS_2, and it represents the performance for a period of infinite duration. The lever rule can be applied to estimate the rates at VSS, CSS, and QSS

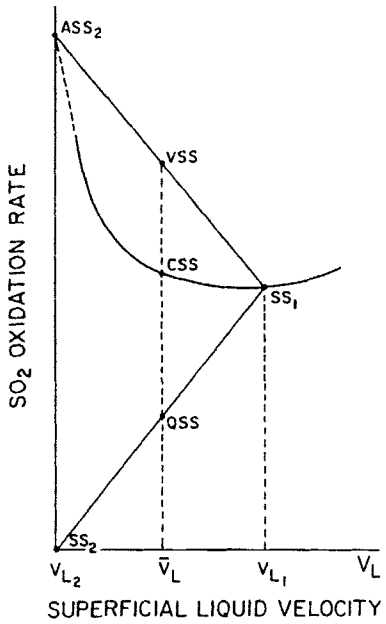

FIG. 20. Schematic diagram showing the estimation of the time-average rate of SO_2 oxidation under periodic flow interruption or reduction employing steady-state oxidation rate vs liquid loading data (Figure from Haure *et al.*, 1989, with permission, © 1989, American Institute of Chemical Engineers.)

for s other than 0.5. Table XII shows that an estimate of the rate of SO_2 oxidation under periodic flow interruption can be obtained from steady-state rate data.

The role of water in SO_2 oxidation over activated carbon is to react with the SO_3 formed to yield sulfuric acid. This removes SO_3 from the catalyst

TABLE XII
PREDICTED[a] VS EXPERIMENTAL SO_2 OXIDATION RATES[b]

Cycle split	Mean superf. liquid, mm/s	CSS	Time avg. VSS	Exp. periodic rate	% diff.[c]
0.5	1.7	67	82	88.7	8
0.5	0.8	80	85	90.8	7
0.25	0.8	80	88	94	7
0.1	0.33	97	97	97.7	1

[a] VSS predicted from steady-state rates using construction shown in Fig. 20.
[b] Oxidation rates: μmol/kg · s.
[c] (Experimental − predicted)/predicted as %.

surface and prevents inhibition of the reaction. Consequently, in the absence of liquid flow as the reaction continues, the acid concentration builds up in the intraparticle liquid and interparticle hold-up. Once liquid flow is restarted, the initial concentration of acid flushed from the bed will be high and will then decay as acid is diluted by water added to the top of the trickle bed. Consequently, a low cycle split and a long period could be used to obtain a high acid concentration. Haure *et al.* varied s and τ and demonstrated that higher sulfuric acid concentrations were obtained. These researchers also examined what acid strength could be obtained starting with a water feed. For this purpose, they conducted a step change experiment and measured the strength of the acid leaving the bed in the first minute of liquid flow after steady-state liquid flow had been halted for a variable length of time. A nearly linear variation of acid molarity with the duration of flow interruption was observed. A molarity of about 1.2 was reached in their experiment. The acid concentration within the catalyst pellets was certainly much higher, possibly reaching 2 to 3 M.

The discrepancy between estimated and measured rates of SO_2 oxidation in Table XII arises, according to Haure *et al.* (1989), because the mean spatial temperature of the trickle bed depends on liquid loading. Flow interruption raises the time-average, space mean bed temperature. Figure 21 illustrates the effect. Time-average temperatures are shown for the three thermocouples located axially along the periphery of the carbon bed for periodic operation. Adjusting the steady-state data for the higher temperature using an activation energy of 10 kJ/mol for O_2 transport brings together the estimated and measured time-average rates of oxidation shown in Table XII.

Temperatures within the trickle bed during flow interruption vary with time in the form of temperature waves which move downward through the bed. Measured temperatures are shown in Fig. 22 as a function of cycle split for $\tau = 60$ min. Time-average superficial liquid velocity is constant for the three experiments at 1.65 mm/s. There are some interesting features of these waves: (1) The temperature of the top thermocouple, located some 30 mm below the top of the carbon bed, decreases prior to water addition; (2) temperature increases rather then decreases when the liquid flow begins if $s < 0.25$; and (3) the lags between the temperature maxima are reasonable for the $s = 0.5$ experiment, but are an order of magnitude longer than the plug flow filling times at the smaller cycle splits. The temperature rise at small s appears to be caused by hotter fluid being forced downward by the entering water after flow starts; heating through acid dilution is much too small at the concentrations encountered in the bed to account for the temperature rise. Cooling of the top thermocouple is caused by inhibition of the reaction as the acid concentration builds up and by evaporation as

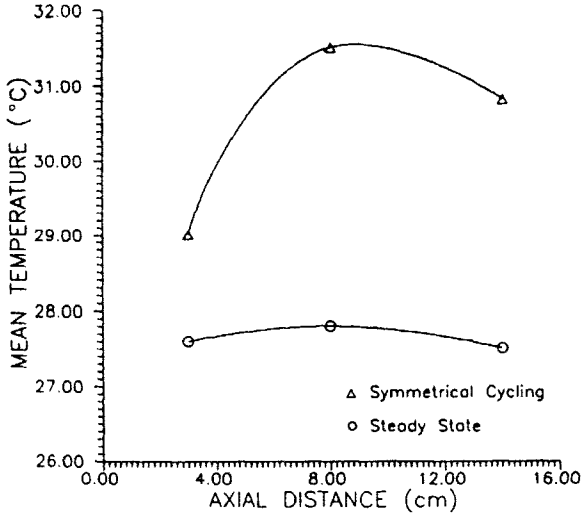

FIG. 21. Comparison of time-average temperature reading from thermocouples located at different axial points on the periphery of the carbon bed for periodic flow interruption and steady-state operation. Time-average u = 1.65 mm/s; for flow interruption, τ = 60 min and s = 0.5. Gas and liquid inlet temperature is about 26.5°C. (Figure from Haure *et al.*, 1989, with permission, © 1989 American Institute of Chemical Engineers.)

dry air enters the carbon bed. The time lags may be caused by poor flow distribution. Changes in peak shape with time suggest that some sort of flow distortion is occurring in the trickle bed.

B. MODELING AND SIMULATION

The model presented in Table XIII was developed (Haure *et al.*, 1990; Stegasov *et al.* 1992) from modeling of phase change in trickle beds (Kirillov and Stegasov, 1988). The model is dynamic, but it neglects the filling and draining steps. These are assumed to occur instantaneously. This assumption has been tested (Hasokowati *et al.*, 1994). The filling step appears to occur as plug flow at the spatial mean liquid velocity in the packing (u_2/ε_{bed}). Even in a bed several meters deep, it is complete in minutes. Gravity drainage, which governs most of the bed, occurs almost as fast as the filling step. However, the bottom of the bed drains by a film thinning mechanism and is much slower, taking perhaps several minutes. Fortunately, the error introduced by neglecting the different static hold-up at the bottom of the trickle bed is small. Thus, the filling and draining steps are not important for beds of several meters in depth unless periods of less

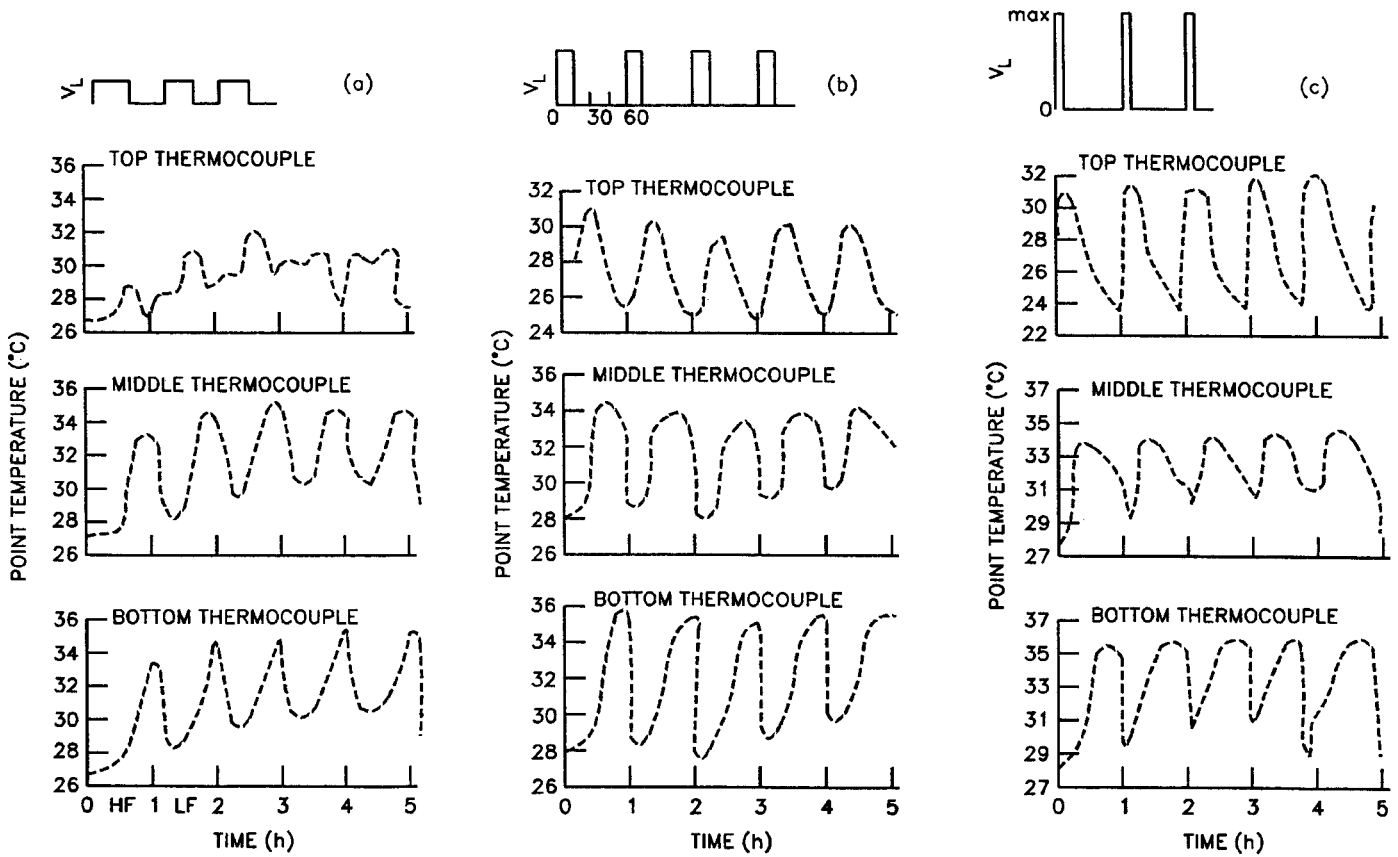

FIG. 22. Thermocouple temperature readings in an experimental trickle bed operating under periodic flow interruption with $\tau = 60$ min and a time-average $u = 1.65$ mm/s: (a) $s = 0.5$, (b) $s = 0.25$, (b) $s = 0.1$. (Figure from Haure *et al.*, 1990, with permission, © 1990 Elsevier Science Publishers.)

TABLE XIII

GENERAL MODEL FOR A PERIODICALLY OPERATED TRICKLE BED (STEGASOV *ET AL.*, 1992)

Heat and material balances

Material balances, Gas (vapor) phase:

$$\alpha_g \rho_g \left[\frac{\partial y_i}{\partial t} + u_g \frac{\partial y_i}{\partial z} \right] = R_i \quad (i = 1, 2) \tag{67}$$

$$\alpha_g \rho_g \left[\frac{\partial y_i}{\partial t} + u_g \frac{\partial y_i}{\partial z} \right] = (R_{evap})_i \quad (i = 3, 4) \tag{68}$$

$$\alpha_g \rho_g \left[\frac{\partial y_i}{\partial t} + u_g \frac{\partial y_i}{\partial z} \right] = 0 \quad (i = 5) \tag{69}$$

Liquid phase:

$$\alpha_l \rho_l \left[\frac{\partial C_i}{\partial t} + u_l \frac{\partial C_i}{\partial z} \right] = R_i + \nu_i R_p \quad (i = 1, 2) \tag{70}$$

$$\alpha_l \rho_l \left[\frac{\partial C_i}{\partial t} + u_l \frac{\partial C_i}{\partial z} \right] = R_{evap} + \nu_i R_p \quad (i = 3, 4) \tag{71}$$

Heat balance equations:

$$\varepsilon (\rho u C_p)_{mix} \frac{\partial T}{\partial z} = h_l(\theta - T) + \varepsilon \sum_{i=1}^{2} R_i H_i - \varepsilon \sum_{i=3}^{4} (R_{evap})_l (\Delta H_{evap})_i \tag{72}$$

$$(1 - \varepsilon)\rho_s (C_p)_s \frac{\partial \theta}{\partial t} = \lambda \frac{\partial^2 \theta}{\partial z^2} - h_l(\theta - T) + R_P \Delta H_R - \varepsilon \sum_{i=1}^{2} R_i H_i + \varepsilon \sum_{i=3}^{4} (R_{evap})_i (\Delta H_{evap})_i \tag{73}$$

Constraints and initial conditions

Equation for variation of liquid phase bulk content:

$$\frac{\partial}{\partial t}(\alpha_l) + \frac{\partial}{\partial z}(\alpha_l u_l) = 0 \tag{74}$$

Equation of state:

$$P = \rho_g \bar{R} T \tag{75}$$

Constraints:

$$\alpha_g + \alpha_l = 1, \quad u_g = \frac{Q_g}{A_x}, \quad u_l = \frac{Q_l}{A_x} \tag{76}$$

Initial and boundary conditions:

At $t = 0$: $\bar{u}(0, z) = \bar{u}^0(z)$, $\theta(0, z) = \theta^0(z)$:

$$\alpha_l(0, z) = \begin{cases} \alpha_g -, & \text{at the start of waterflow} \\ \alpha_g + \alpha_d, & \text{at the cut off of waterflow} \end{cases} \tag{77}$$

At $z = 0$; $\bar{u}(t, 0) = \bar{u}_0(t)$, $\dfrac{\partial \theta}{\partial z} = 0$, (78)

$$\alpha_l(t, 0) = \begin{cases} \alpha_g + \alpha_d -, & \text{at the start of waterflow} \\ \alpha_g -, & \text{at the cut off of waterflow} \end{cases} \tag{79}$$

At $z = L$: $\dfrac{\partial \theta}{\partial z} = 0$ (80)

than 30 min are used. As may be seen in the table, the model is one-dimensional and thus assumes perfect liquid and gas distribution in the carbon bed and negligible radial heat loss. Plug flow of both phases is assumed. Interphase transport of all but sulfuric acid is allowed. Diffusion in and out of the carbon pellet is accounted for by an effectiveness factor.

A well-substantiated correlation for air–water systems taken from the trickle bed literature (Morsi and Charpentier, 1981) was used for the volumetric mass transfer coefficients in the R_i and $(R_{evap})_i$ terms in the model. The h_i term was taken from a correlation of Kirillov *et al.* (1983), while the liquid hold-up term α_l in Eqs. (70), (71), (74), (77), and (79) were estimated from a hold-up model of Specchia and Baldi (1977). All of these correlations require the pressure drop per unit bed length. The correlation of Rao and Drinkenburg (1985) was employed for this purpose. Liquid static hold-up was assumed invariate and a literature value was used. Gas hold-up was obtained by difference using the bed porosity.

Stegasov *et al.* (1992) expressed the kinetic rate of SO_2 oxidation as

$$R_p = \frac{\nu_4 k_2 \eta \eta_o C_1 C_2}{1 + AC_4}, \tag{81}$$

where C_1, C_2, and C_4 are the liquid-phase concentrations of SO_2, O_2 and H_2SO_4, respectively. The kinetic rate constant, k_2, the effectiveness factor, η, and the constant A in the denominator were taken from Komiyama and Smith (1975). Haure *et al.* (1989) were able to closely predict their steady-state measurements using these data. Stegasov *et al.* chose the wetting efficiency (η_o) function to fit the line representing Haure's steady-state data, but demonstrated that the function used agreed closely with wetting efficiency correlations proposed in the literature. Essentially, then, Table XIII is an apriori model.

For integration, Stegasov *et al.* approximate the equations in Table XIII by forward differences, which provides at each grid point a set of implicit algebraic equations that must be solved. The Runge–Kutta procedure was used for solution of temperature distribution in the bed and then an iterative procedure was used to find concentrations at the $n + 1$ time step. Time step was variable and was optimized continually during integration. A Richardson-type improvement was also used (Stegasov *et al.*, 1992).

Figure 23 shows a simulation of Haure's periodic flow interruption data at time-average $u = 0.86$ mm/s (Curves 1 and 1′) and $u = 1.65$ mm/s (Curves 2 and 2′). Data points and the fit (dashed line) are from Fig. 19. The simulation predictions are 28 to 35% too high, which is not bad considering the 25% variation in the experimental data shown in Fig. 19. The trends, however, are not properly represented. Figure 23 predicts enhancement factors declining with τ, whereas data indicate an increase at low τ and

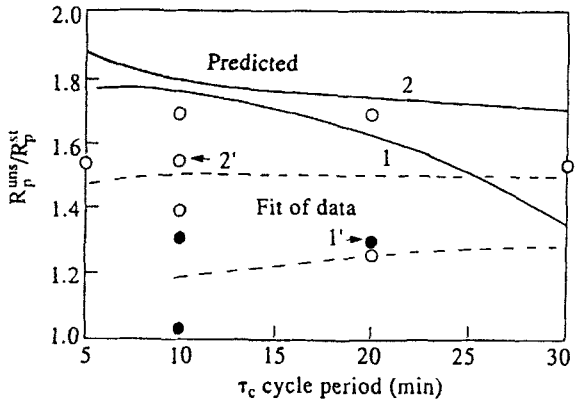

FIG. 23. Comparison of predicted and experimental enhancement factors for the experimental conditions of Fig. 19. Curves designated 1 and 1′ are for v_L = 0.86 mm/s, while curves 2 and 2′ are for v_L = 1.65 mm/s. The prime designates the data fits in Fig. 19. (Figure from Stegasov *et al.*, 1992, with permission, © 1992 Elsevier Science Publishers.)

then no effect of period as τ augments. Improper estimate of the trend with period is traceable to two considerations: (1) At periods below 10 min the draining time of the bed cannot be neglected, and (2) the inhibition effect of acid buildup in the bed under zero water flow seems overpredicted.

The Stegasov *et al.* model does a much better job of predicting the effect of cycle split on time-average acid concentration leaving the trickle bed. Figure 24 shows that the model prediction for v_L = 1.65 mm/s and τ =

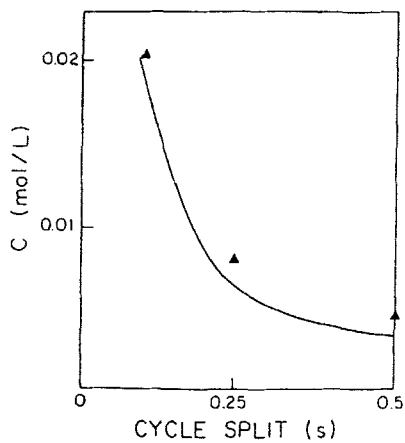

FIG. 24. Comparison of predicted and experimental time-average acid concentrations leaving the periodically operated trickle bed for the experimental conditions of Fig. 19 and τ = 10 min. (Figure from Stegasov *et al.*, 1992, with permission, © 1992 Elsevier Science Publishers.)

10 min agrees well with experimental data. However, prediction of the thermocouple data given in Fig. 22 was poor. Temperatures are overpredicted at $s = 0.25$ and particularly at $s = 0.1$, but the increasing temperature observed from the top to bottom thermocouples is properly represented. At $s = 0.5$, the temperatures and the increase from top to bottom seen in the data are well predicted. Indeed, the model predicts the constant temperature during the water flush, the temperature rise after water flow is discontinued, and the sharp drop when the water flow commences for the middle and bottom thermocouples at $s = 0.5$. The simulation poorly reproduces the behavior of the top thermocouple, but that temperature–time record is so irregular that the data are suspect. With respect to the data in Fig. 22 for $s = 0.1$, the simulation fails to predict the shape of the temperature–time record. It also fails to predict the drop in temperature prior to restart of liquid flow, and it predicts a short constant-temperature period when experimentally none is observed.

Some of the poor agreement is undoubtedly attributable to the data. Measurements were made at the periphery of the bed where radial heat loss becomes important. Certainly this contributes to the poor agreement at $s = 0.1$ when temperatures are highest in the bed. The Stegasov model assumes no radial gradients. If allowance is made for an a priori model with no data fitting, not even for reaction rate constants, then the performance is quite good. Certainly, tuning of the rate and mass transfer coefficients should improve the agreement of model and data in Fig. 23. Consequently, it is evident that periodic flow interruption can be modeled. The model proposed by Stegasov *et al.* (1992) will be useful for data interpretation and for scale-up of experimental results.

A useful application of the model is to examine the SO_2 and O_2 concentration profiles in the trickle bed. These are shown for the steady-state conditions used by Haure *et al.* (1989) in Fig. 25. The equilibrium SO_2 concentration drops through the bed, but the O_2 concentration is constant. In Haure's experiments O_2 partial pressure is 16 times the SO_2 partial pressure. At the catalyst particle surface, however, O_2 concentration is much smaller and is only about one-third of the SO_2 concentration. This explains why O_2 transport is rate limiting and why experimentally oxidation appears to be zero-order in SO_2.

C. Application to Stack-Gas Scrubbing

Several papers describe extension of the Haure work to the scrubbing of industrial stack gases as one step of a carbon based stack-gas cleanup process referred to as the RTI–Waterloo Process (Gangwal *et al.*, 1992;

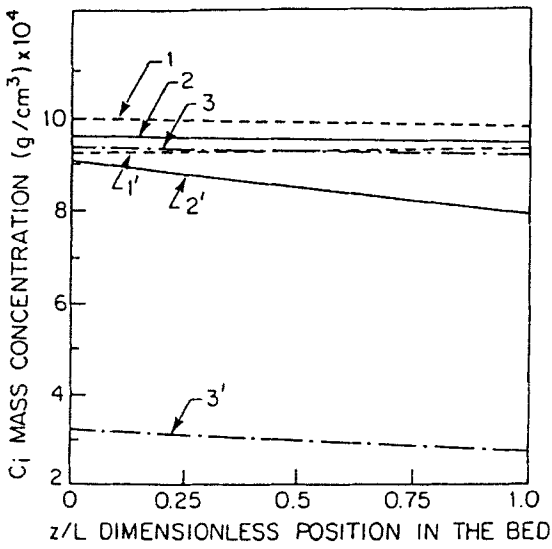

FIG. 25. Predicted mass concentration profiles for SO_2 and O_2 in the experimental trickle bed used by Haure *et al.* (1989) at v_L = 1.65 mm/s. (Figure from Stegasov *et al.*, 1992, with permission, © 1992 Elsevier Science Publishers.)

Metzinger *et al.*, 1992; 1994; Lee *et al.*, 1995, 1996a,b). Figure 26 provides a schematic of the process as conceived for stack gas from a coal burning power plant using an Illinois #6 coal containing 2.8 wt% sulfur. Hot gas leaving an electrostatic precipitator is cooled by gas–gas heat exchange to a temperature just above the boiling point of the product acid and enters a trickle bed. With a sufficient depth of the carbon bed, SO_2 removal and conversion to sulfuric acid is between 98 and 99%. By washing the carbon bed with product acid in place of water, a 5 to 10 N acid can be made, even with some water condensation. Acid leaves the bottom of the bed and the stream is split. Some flows to product storage, while the remainder is diluted with water and is recycled to flush the carbon bed. Although space velocities up to 10,000 h^{-1} seem feasible, several beds in parallel will be needed for satisfactory liquid distribution. Acid flow is continuous; the flow, however, is switched periodically from bed to bed. The wet but desulfurized gas is reheated in the gas heat exchanger before entering the SCR deNO_x unit. With the very low level of SO_2 achieved in the scrubber, precipitation of ammonium sulfite/sulfate in the SCR can be avoided.

The attraction of periodic flow interruption for scrubbing is that the pressure drop is low relative to continuous, packed-bed scrubbers and a commercially useful acid can be produced. The catalyst is cheap, but that

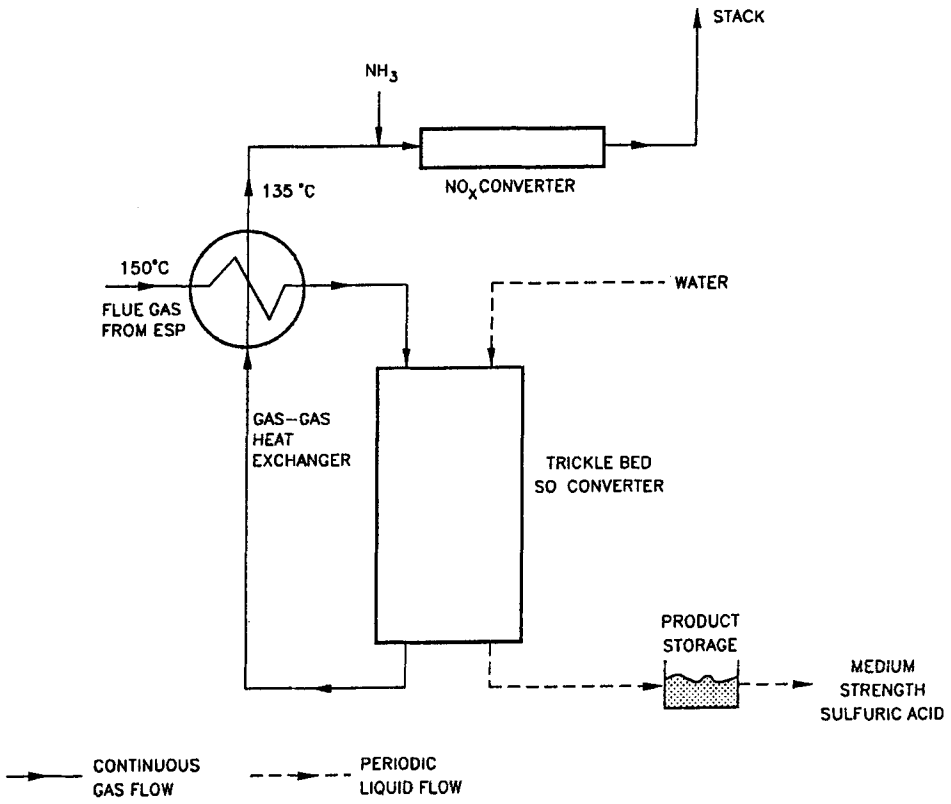

FIG. 26. Process flowsheet for the RTI–Waterloo process for stack-gas cleanup for coal burning power plants. (Figure taken from Gangwal *et al.*, 1992, with permission of the authors.)

is not a serious consideration, because laboratory experiments indicate that the carbon can be used for long periods.

The first set of experiments on SO_2 scrubbing used a series of step on and off experiments to test the performance of candidate carbons. Flooding the ca. 1-m deep bed of the test carbon with water or acid of different strength for an extended time period was followed by draining the bed and introducing simulated stack gas (600 to 2500 ppmv SO_2, 0 to 500 ppmv NO_x, 5 vol% O_2, 15 vol% CO_2, and 2 to 10 vol% H_2O). Gas flow was discontinued when breakthrough occurred and the cycle was repeated. Breakthrough was defined as the condition when SO_2 leaving the bed reached 5% of the inlet concentration. Different activated carbons displayed different breakthrough behavior, indicating that the choice of carbon is important. One carbon exhibited rate inhibition at 2500 ppmv SO_2 in the feed. All carbons showed a decrease in breakthrough time when 4.3 N acid

replaced water as the flushing liquid. Adding a noble metal promoter to the carbon extended breakthrough time, while raising the operating temperature from 80 to 130°C sharply reduced the breakthrough time. Gangwal *et al.* (1992) give further experimental details.

Further experiments were carried out in the equipment shown in Fig. 18. Some important changes were made. Gas mixing was added to provide a simulated stack gas. Moisture level was adjusted either with a saturator or by adding live steam. The liquid side of the system was constructed entirely of glass so acid strengths up to 10 N could be used. Thermocouples were mounted radially as well as axially and could be inserted to variable depths into the bed. Finally, an SO_2 detector was placed in the off-gas line following the separator at the bottom of bed. Steady-state and periodic flow interruption measurements with the modified equipment are reported by Metzinger *et al.* (1994) for the BPL activated carbon and for a noble-metal-impregnated carbon. Since the bed depth of the experimental trickle bed was just 180 mm, breakthrough was not observed.

The dependence of SO_2 removal and SO_2 conversion to sulfuric acid on operating conditions is shown in Fig. 27 for experiments carried out at a bed temperature of 21°C using water as the flushing fluid. Steady-state measurements are also shown. Contrary to the results of Haure *et al.* (1989), periodic interruption of the liquid flow did not increase SO_2 removal at SV = 1000 h^{-1}; however, removal and conversion to acid at SV = 3000 h^{-1} was more than twice the steady-state values. As expected, gas space velocity is important. Removal drops as SV increases. The figure shows that washing the carbon bed with 2 N acid suppresses SO_2 removal, but has only a small effect on conversion to acid. A flush duration, D, of 3 min is significantly better than a 30-s duration and higher removals and conversion are found when $\tau = 5$ min rather than 30 min. Only about 50% of the SO_2 absorbed is converted to H_2SO_4 at high levels of removal; however, at higher SVs the percentage becomes about 70%. Consequently, unconverted SO_2 is present in the liquid phase as sulfurous acid or dissolved SO_2. These results came from a $2^5 - 1$ factorial experimental design that was used to identify system variables with the largest impact on SO_2 removal, conversion, and pressure drop over the bed. Measurements were made once flow interruption reached a stationary condition, that is, the variation with time of the SO_2 concentration leaving the bed during the zero liquid flow portion of the cycle was reproducible.

A less comprehensive factorial design was used at 80°C. Flush duration and τ were not considered. Very little sulfurous acid or dissolved SO_2 were found in the liquid collected, so conversion to acid is essentially the same as SO_2 removal. Figure 28 plots percent removal vs the normality of the wash liquid. Increasing normality lowers the percent SO_2 scrubbed from

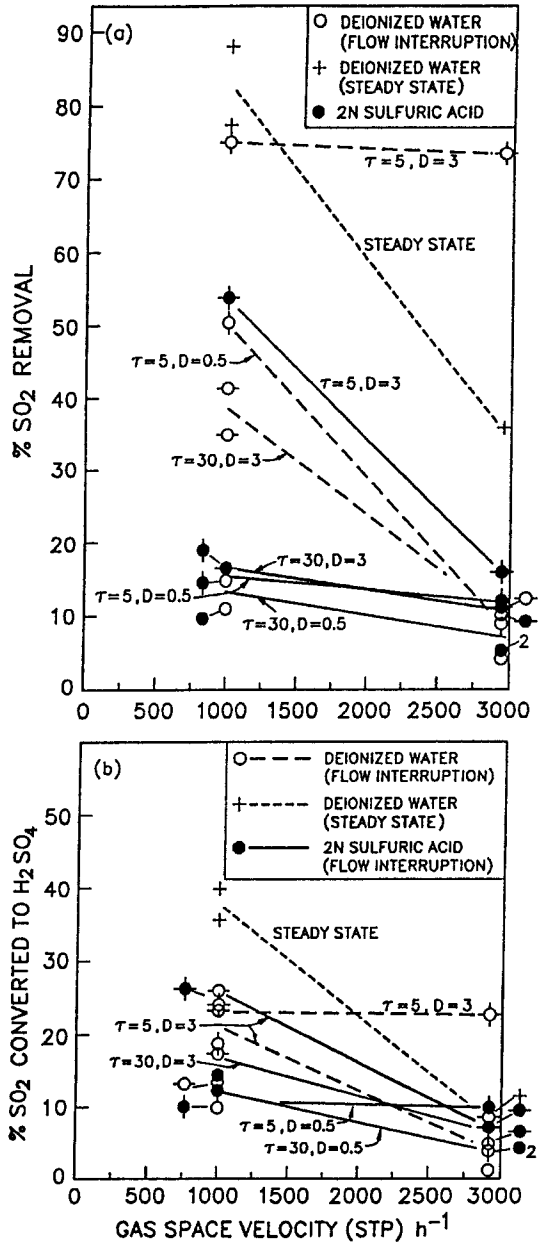

FIG. 27. Effect of space velocity, cycle period, normality of the flushing liquid, and flush duration on SO_2 scrubbing from a simulated stack gas at 21°C employing a bed of BPL carbon: (a) SO_2 removal, (b) SO_2 conversion to H_2SO_4. (Figure reproduced from Metzinger *et al.*, 1994, with permission, © 1994 Elsevier Science Ltd.)

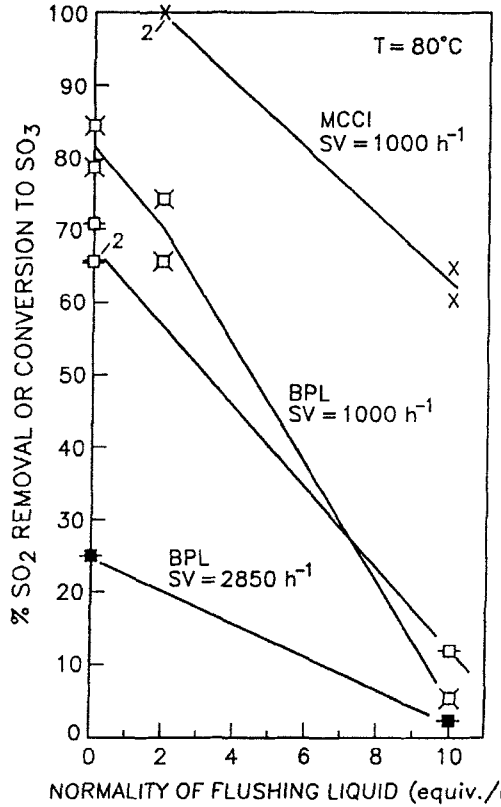

FIG. 28. Effect of acid strength, space velocity, and activated carbon on SO_2 removal and conversion to acid at 80°C in an intermittantly flushed trickle bed for τ = 60 min and s = 0.1. (Figure reproduced from Metzinger *et al.*, 1994, with permission, © 1994 Elsevier Science Ltd.)

the stack gas. The MCCI carbon, impregnated with a noble metal, provides far better SO_2 removal than the BPL carbon. Indeed, it appears a bed of this activated carbon could produce a 10 N H_2SO_4 from 2500 ppm SO_2 in a typical stack gas from a high-sulfur coal. Space velocity continues to exert a strong influence on removal at 80°C.

Assuming plug flow of both phases in the trickle bed, a volumetric mass transfer coefficient, $k_L a$, was calculated from the measurements. The same plug flow model was then used to estimate bed depth necessary for 95% SO_2 removal from the simulated stack gas. Conversion to sulfuric acid was handled in the same way, by calculating an apparent first-order rate constant and then estimating conversion to acid at the bed depth needed for 95% SO_2 removal. Pressure drop was predicted for this bed depth by multiplying

the depth by the experimental pressure drop per unit bed depth. Bed depths and anticipated pressure drops for a portion of the experiments are collected in Table XIV. The table shows that low pressure drops can be achieved at 95% SO_2 removal only at 80°C provided acid strength does not exceed 10 N and SV = 1000 h^{-1} is acceptable. Because of the large flows encountered in power plants, space velocity of 10,000 h^{-1} or more will be needed. In this case, pressure drops will be more than 100 times those given in the last column of Table XIV, as pressure drop increases with the square of the velocity. Pressure drops greater than 50 kPa will require placing a blower in the stack, greatly increasing the cost of SO_2 removal.

A systematic study of the cycling variables, cycle period (τ), flush duration (D) or cycle split (s), and the liquid loading (u_l) for the poorer performing BPL activated carbon is reported by Lee *et al.* (1995). All their measurements were undertaken at 80°C. Contrary to the influence of period seen in Fig. 27, Lee *et al.* observed that SO_2 removal and conversion to acid increase as τ augments while holding s constant. Results of this study are summarized in Fig. 29. The middle figure suggests there is an optimum

TABLE XIV
ESTIMATED CARBON BED DEPTH AND PRESSURE DROP AT 95% SO_2 REMOVAL[a]

Catalyst temperature, flush liquid, space velocity	SO_2 removal in 190 mm deep bed (%)	Bed depth for 95% SO_2 removal (m)	Pressure drop at 95% SO_2 removal (kPa)
BPL—Activated Carbon			
21[a]/water			
SV = 1000 h^{-1}	38	1.19	0.84
= 2850	10	5.36	3.75
21[a]/2 N acid			
SV = 1000 h^{-1}	16	3.20	21
= 2850	11	4.98	68
80[a]/water			
SV = 1000 h^{-1}	67 (80)	0.270 (0.224)	0.71 (0.59)
= 2850	26	0.70	1.85
80[a]/2 N acid			
SV = 1000 h^{-1}	70	0.258	0.68
80[a]/10 N acid			
SV = 1000 h^{-1}	12 (6)	146 (3.0)	19 (24)
= 2850	2.4	7.68	101
MCCI—Impregn. Carbon			
Acid			
SV = 1000 h^{-1}	(100)	(0.18)	(1.7)
80[a]/10 N acid			
SV = 1000 h^{-1}	(60)	(0.30)	(4.0)

[a] Values in parentheses means τ = 60 min rather than 30 min.

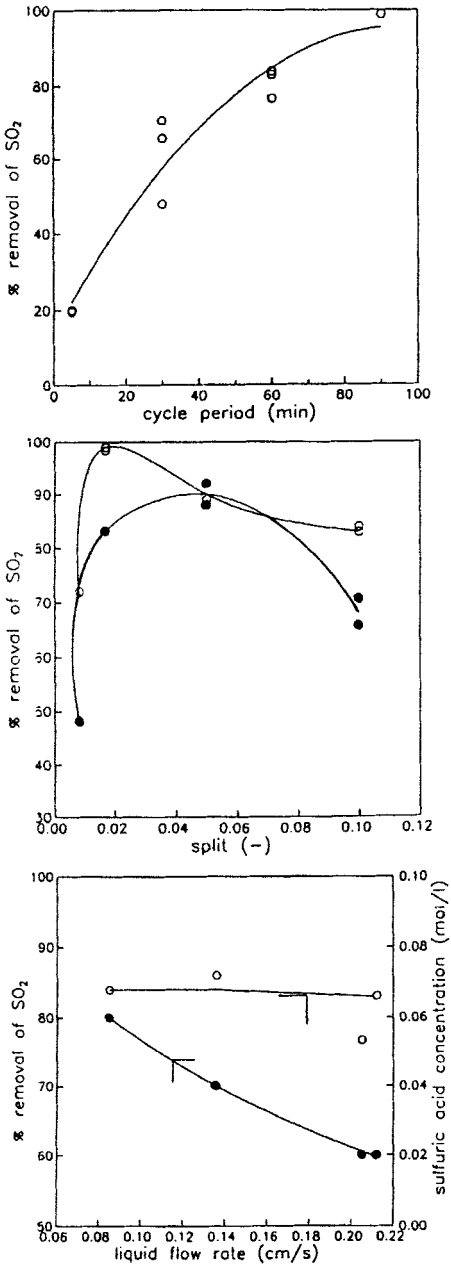

FIG. 29. Dependence of SO_2 removal on cycling variables using BPL activated carbon with gas and liquid feed temperatures at 80°C and a gas SV = 1000 h^{-1}: (a) influence of τ at s = 0.1 and u_l between 0.085 and 0.212 cm/s, (b) influence of s at τ (○ = 60 min, ● = 30 min) and u_l between 0.059 and 0.212 cm/s, (c) influence of u_l at τ = 60 min and s = 0.1. (Figure reproduced from Lee *et al.*, 1995, with permission, © 1995 Elsevier Science Ltd.)

cycle split, which depends on τ. Unfortunately, Fig. 29 does not isolate the dependence of scrubbing performance on flush duration. The duration, D, at any τ changes as s varies in (b). This is also true in (a): D increases in step with τ. The bottom figure shows that SO_2 removal is unaffected by u_l at $\tau = 60$ min and $s = 0.1$. Of course, increasing the liquid loading during washing of the carbon bed dilutes the acid formed.

In a follow up study, Lee *et al.* (1996a) returned to the choice of activated carbon for the scrubbing process. A new activated carbon, Centaur (Calgon Carbon Corp.), was tested under condition used for Lee's earlier work discussed in the previous paragraph. Levels of SO_2 removal approaching 99% were obtained with a 180-mm deep bed at 80°C and SV = 1000 h^{-1} with this carbon. Impregnating the carbon with Pt at a 0.1 wt% loading did not increase the SO_2 removed. Evidently, impregnation with noble metals is not needed to achieve high activity for SO_2 oxidation. Figure 30 shows percent SO_2 removal from stack gas as a function of cycle split and period for BPL and Centaur activated carbons. The figure suggests that for both carbons there is a minimum s or actually D for high SO_2 removal. Results for the Centaur carbon did not indicate an optimum s or D.

D. Physical Explanation

The success of periodic flow interruption is due to the liquid static hold-up within the porous catalyst pellets and the interstices of the catalyst bed.

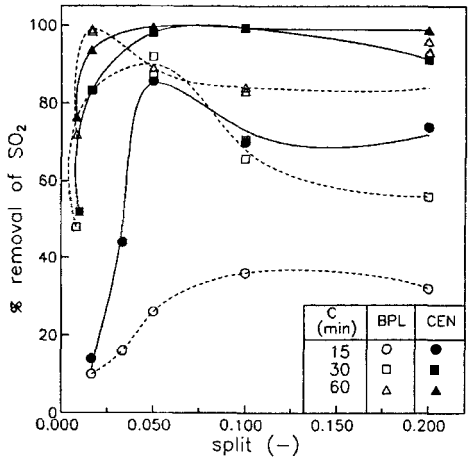

FIG. 30. Dependence of SO_2 removal on cycle split and period for a 178-g bed of either Centaur or BPL activated carbon with gas and liquid feed temperatures at 80°C, SV = 1000 h^{-1}, and u_l = 0.2 cm/s. (Figure reproduced from Lee *et al.*, 1996a, with permission of the authors.)

Thus, the liquid continues to be present even though it is no longer flowing through the bed. It is the dynamic hold-up that varies through this form of periodic operation. When this hold-up diminishes, the mass transfer resistance for the gas phase reactant decreases and the rate of reaction rises. The role of the liquid flow portion of the cycle then is to recharge the internal particle and the interstitial static hold-up and to carry away the reaction products. It is the latter role that is important in SO_2 oxidation because the buildup of acid reduces gas solubility and inhibits the rate of oxidation. The negative effect of acid concentration on SO_2 oxidation, and thus removal from the stack gas, is illustrated in Fig. 27. The liquid phase also removes the heat released by the chemical reaction. The temperature rise with zero liquid flow contributes importantly to the higher rates measured by Haure *et al.* (1989) for SO_2 oxidation under periodic operation. It is less important in the stack gas application because the SO_2 concentration is much smaller. Stack gas is not saturated with water vapor, so a more important effect is cooling of the bed through evaporation.

In a trickle bed with intermittent liquid flow and significant static hold-up, cooling through evaporation, heating due to reaction, solubility changes with temperature and acid concentration, and mass transfer changes on flow interruption lead to complex and changing levels of SO_2 removal and bed temperatures within a cycle. These are illustrated in Fig. 31, which presents measurements for the Centaur carbon at 80°C. Narrow vertical bars in the figure show the duration of liquid flow through the carbon bed. The SO_2 detector is located downstream of the trickle bed and the plot does not allow for the time lag. Nevertheless, the rise in SO_2 concentration begins when water is reintroduced. This appears to be a mass transfer effect, because bed temperature increases at the same time. The increase in SO_2 leaving the bed continues after the liquid flow ceases because evaporation cools the bed and decreases the rate of conversion to acid. Early in the cycle, most of the SO_2 is extracted in the upper portion of the carbon bed. About halfway through the cycle, the top of the bed becomes saturated with H_2SO_4 and the reaction ceases. Lower sections of the bed begin to participate to a greater extent in SO_2 removal and oxidation. Temperatures are lower and solubilities are higher, so the reaction rate increases, causing SO_2 in the outlet to drop. Meanwhile, evaporation has halted at the top of the bed and hotter entering gas begins to heat the bed (Fig. 31b).

The pattern shown in Fig. 31 is similar to that observed with BPL carbon, except that the peak reached after water is introduced and then cut off is narrow and climbs to about half of the SO_2 concentration in the feed. If the flush duration is 30 s, bed temperatures tend to be constant and the lowest level of SO_2 in the outlet occurs before water is admitted to the bed. This results in two SO_2 peaks within a cycle.

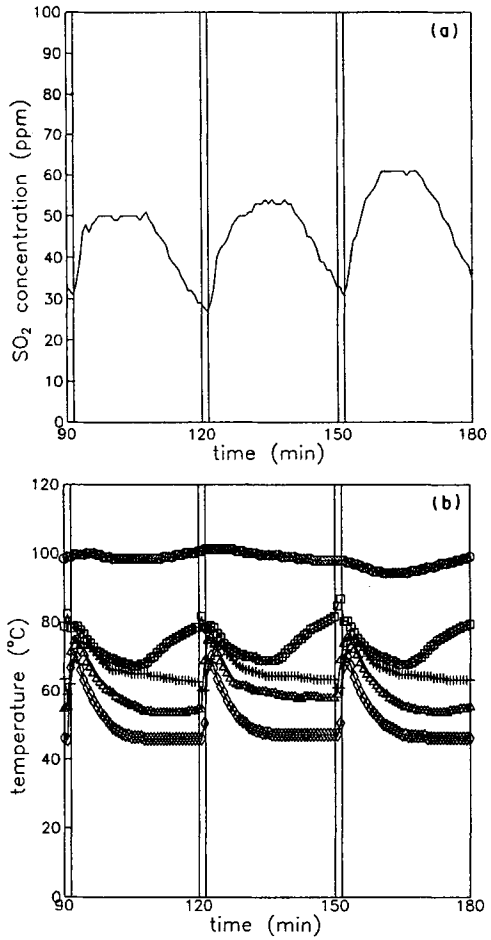

FIG. 31. Variation of outlet SO_2 concentration in ppm (vol) and bed temperatures at different locations within the carbon bed during a cycle. Measurements are for the Centaur carbon with gas and liquid feed temperatures = 80°C and gas SV = 1000 h^{-1}. Cycling variables were τ = 30 min, D = 1.5 min, and u_l = 0.17 cm/s. Symbols: ○ = top of bed, r = 0; □ = middle of bed, r = R; Δ = middle of bed, r = R/2; ◇ = middle of bed, r = 0; + = bottom of bed, r = 0. (Figure reproduced from Lee *et al.*, 1996b, with permission of the authors.)

The preceeding considerations suggest some requirements for rate or conversion improvement through periodic flow interruption in trickle beds: (1) wetting of the catalyst surface by the liquid phase, (2) significant liquid hold-up either interstitially or within the porous catalyst, (3) high liquid loading during the liquid flow portion of a cycle to ensure complete wetting of bed particles, (4) a sufficient duration of liquid flow

to replenish internal and static hold-up, and (5) reaction and operating conditions such that mass transfer of a gas-phase reactant either is rate limiting or is one of the slower steps in the reaction-transport network. For the stack-gas scrubbing application, it is the duration of the liquid flush that is crucial to performance.

V. The Future of Periodic Operations for SO_2 Oxidation

The multistage catalytic converter used when sulfuric acid is produced by burning sulfur or from a hot smelter discharge with a moderately high SO_2 content represents fully developed, low-cost technology. It seems unlikely that a periodically operating process will displace this continuous process. Thus, the different ways of using periodic operation we have examined in this review seem relegated to special situations.

With respect to periodic reversal of flow direction, this seems to be competitive for low levels of smelter gas SO_2, probably under 4 vol%, at ambient temperature. If SO_2 is too high, thermal runaway can occur. A second, important application is to reduce SO_2 in the off-gas from a conventional acid plant. Use of flow reversal avoids the problem of reheating the gas leaving the first-stage absorber.

As for periodic air blowing of the final stage of a converter, this seems also to be technology for a special situation. It is a method of reducing SO_2 emissions to the environment, and thus it competes with periodic reversal of flow direction. It is not clear which of the two gives the better performance. Periodic flow reversal is a simple add-on at the tail end of a plant. Periodic air blowing, on the other hand, involves modification of a converter such as doubling the final stage and putting in piping to bring hot air from this stage to the primary and secondary air inlets of the sulfur burner. Modifications required can be seen from Fig. 4.

Periodic air blowing requires further development. For one, it has not been optimized with respect to cycle variables. The technology also needs to be tested on a pilot scale. Unlike periodic flow reversal, periodic air blowing requires a rapid-action three-way valve that will be exposed to SO_2 and SO_3 at temperatures between 350 and 400°C. Both flow reversal and air blowing subject the catalyst to significant periodic swings in temperature that may influence catalyst life. Data on catalyst life is not available. Nieken *et al.* (1994) and Budman *et al.* (1996) have pointed out that reactors incorporating periodic reversal of flow direction exhibit high parametric sensitivity, that is, an upward shift in SO_2 concentration could lead to

thermal runaway, while a reduction in concentration may extinguish the reaction. Suitable control strategies for SO_2 oxidation need development.

Periodic interruption of liquid flow in a trickle-bed scrubber is another technology for special situations. It is directed at parts-per-million levels of SO_2 and probably cannot compete with conventional technology or other periodic operations, because it produces acid at a low concentration. Even though the carbon-based, periodic flow interruption process seems to be the most economic scrubbing process for 95% SO_2 removal (Gangwal *et al.,* 1992), that process, too, seems destined only for special applications. Fuel desulfurization is certainly the most economical method of reducing SO_2 emissions from power stations. Lime injection into the fire zone seems to be the favored route for coal-based plants, or, when higher levels of SO_2 removal are needed, scrubbing with a lime solution in a spray tower can be used. Thus, scrubbing seems limited to industrial discharges, such as emissions from acid plants where lime injection cannot be used. It may also have an application as a tail-end process for power-plant stack gases. Lime injection appears to be limited to 75 to 85% SO_2 removal at reasonable levels of lime addition, and scrubbing with a lime solution produces a solid waste.

Several uncertainties in this periodic process have not been resolved. Pressure drop is too high at SV = 10,000 h^{-1} when packed beds of carbon are used. Study of carbon-coated structured packing or of monoliths with activated carbon washcoats is needed to see if lower pressure drops at 95% SO_2 removal can be achieved. Stack gas from coal or heavy oil combustion contains parts-per-million or -per-billion quantities of toxic elements and compounds. Their removal in the periodically operated trickle bed must be examined, as well as the effect of these elements on acid quality. So far, laboratory experiments have been done to just 80°C; use of acid for flushing the carbon bed should permit operation at temperatures up to 150°C. Performance of periodic flow interruption at such temperatures needs to be determined. The heat exchange requirements for the RTI–Waterloo process shown in Fig. 26 depend on the temperature of SO_2 scrubbing. If operation at 150°C is possible, gas leaving the trickle bed can be passed directly to the deNO$_x$ step without reheating.

Nomenclature

ASS	apparent steady state
A_x	cross-sectional area (m^2)
a	volume specific interfacial area (m^{-1})

a_g geometric specific surface area
B dimensionless activation energy
CSS steady state at the time-average liquid superficial velocity
C concentration (mol/m^3)
C_i concentration of the ith species
concentration of the ith species in the liquid phase (Table XIII)
C_j concentration of the jth species in the melt (Table XI)
C_v concentration in the melt
C_o maximum concentration of SO_3 in the melt phase
C^o total concentration of pyrosulfate and sulfate anions
C_v concentration of biatomic vanadium complexes
C_3^L concentration of SO_3 in the melt phase
C_p specific heat (kcal/kg °C)
C_r ratio of solid to gas heat capacities [dimensionless—see just after Eq. (49)]
c_p specific heat (kcal/kg °C)
D dissymmetry factor (dimensionless)
duration of flushing (min)
D_e effective diffusion coefficient (m^2/s)
D_i axial dispersion coefficient for species i (m^2/s)
diffusion coefficient of species i mixture (m^2/s)
d particle diameter (m)
d_e equivalent particle diameter (m)
E_k activation energy for the k reaction ($-k$ for the reverse reaction) (kcal/mol)
g acceleration of gravity (m/s^2)
H_i Henry's law constant for species i (mol/m^3 bar)
enthalpy of component i (kcal/mol)
H_j heat of the jth reaction (kcal/mol)
Henry's law constant for species j (Table XI)
H_{in} heat effect on active to inactive transformation (kcal/mol)
H^{dis} heat of solution (kcal/mol)
ΔH heat of reaction
ΔH_{evap} heat of vaporization
h heat transfer coefficient (kcal/m^2 °C s)
h_l liquid particle heat transfer coefficient (kcal/m^2 °C s)
h_p fluid–particle heat transfer coefficient (kcal/cm^3 °C s)
h_w bed-to-wall heat transfer coefficient (kcal/cm^3 °C s)
K equilibrium constant
K_{ad} adsorption equilibrium constant
$(K_L)_k$ equilibrium constant in the melt for the kth reaction (various units)

K_H	solubility constant (mol/cm^3 bar)
k	rate constant
k_k	rate constant for the kth forward reaction
k_k	rate constant for the kth backward reaction
$k_L a$	volumetric mass transfer coefficient (s^{-1})
k_m	transport coefficient from pore volume to melt phase (mol/m^2 s)
k_p	fluid–particle mass transfer coefficient (m/s)
L	length of catalyst bed (cm, m)
n	index integer
P	pressure (bar, kPa)
P_i	partial pressure of species i (bar, kPa)
ΔP	pressure drop (bar, kPa)
Pe_H	Péclet number for heat
Pe_M	Péclet number for mass
Phg	modified Bodenstein number for gas phase (dimensionless—see just after Eqn. [49])
Phs	modified Bodenstein number for solid phase (dimensionless—see just after Eqn. [49])
Q	volumetric flow rate (m^3/s)
R	gas constant (various units)
R_i	rate of mass transfer of species i (kg/m^3 s)
R_p	rate of reaction (kg/m^3 s)
R_{evap}	evaporation rate
r	rate of reaction
r_j	rate of the jth reaction
r_{qss}	quasi-steady-state rate
QSS	quasi steady state
S	specific surface area (various units)
SS	steady state
SV	space velocity (s^{-1}, h^{-1})
STP	standard temperature and pressure
S_m	specific surface are of the melt phase on bed volume basis (m^{-1})
S_v	volumetric specific surface area (m^{-1})
S_{ext}	external surface
s	cycle split
s^v	complex density (mol/cm^3)
T	temperature (°C, K) gas temperature (Tables XI, XIII) dimensionless gas temperature
ΔT_D	model parameter [$H^{dis}/(\rho C_p)_g V_o$, Table XI]
ΔT_i	model parameter [$H_j/(\rho C_p)_g V_o$, Table XI]
ΔT_{ad}	adiabatic temperature rise (°C)

t time (min)
t space time (s)
t_c cycle period (s, min Table XIII)
u superficial velocity (m/s)
u_l superficial velocity of the liquid (m/s, cm/s)
u_L liquid interstitial velocity (m/s)
u_T total interstitial velocity (m/s)
VSS virtual steady state
V_o molar gas volume (22.4 L/mol, Table XIII)
v_L liquid superficial velocity (m/s)
v_{sv} average velocity
X conversion
X_1, X_2 conversion in the upflow(1) and downflow (2) directions in periodic flow reversal
x_i mole fraction of i in the melt phase
x conversion
y_i gas phase mass fraction
y_j mole or mass fraction of complex j in melt phase
y adsorbate conversion
z axial position (cm, m)

Greek

α heat transfer parameter [dimensionless—see just after Eq. (49)]
model parameter [$h_p S v \tau_s/(\rho C_p)_g$, Table XI]
volume fraction or holdup expressed as a bed fraction (Table XIII)
β equilibrium term defined by Eq. (58)
β_j model parameter [$(k_p)_j S_v V_o P_{\pi s}/RT$, Table XI]
β_1 heat generation coefficient [dimensionless—see just after Eq. (49)]
β_2 generation term coefficient [dimensionless—see just after Eq. (49)]
γ parameter [$\alpha(\rho C_p)_g$] dimensionless mass transfer coefficient—see just after Eq. (49)
γ_D model parameter ($2\varepsilon_m \tau_s V_o/\tau$, Table XI)
γ_θ $(\rho C_p)_p)(1_{-\varepsilon B})\tau_s/(\rho C_p)_g\ \tau$
γ_v model parameter ($2/\tau$, Table XI)
ε void fraction
ε_B void fraction in bed
ε_g gas hold-up as fraction of bed volume ()
ε_p void fraction in catalyst particle
ε_m fraction occupied by the melt phase

Θ	temperature of solid (K in Table XI)
θ	dimensionless solid temperature $(1-T_s/T_o)$
	solid temperature (Table XIII)
	dimensionless melt species concentration
$\Delta\theta_{ad}$	dimensionless adiabatic temperature rise
η	overall effectiveness factor
Λ	model parameter ($\varepsilon_m\tau_s C_v V_o$, Table XIII)
λ	conductivity
λ_l	axial conductivity (kcal/m$^{2\circ}$C s)
μ_{jk}	stoichiometric coefficient for component j in the melt for the kth reaction
ν_{ik}	stoichiometric coefficient for species i in the kth reaction
ξ	dimensionless axial position
ρ	density (kg/m^3)
ρ_{cat}	catalyst density (kg/m^3)
ρ_g	gas density (kg/m^3)
τ	cycle period (s, min)
	dimensionless time (Table XI)
τ_s	space time (s, min)
τ'	dimensionless time (t/τ_s)
$\tau_{1/2}$	half cycle time (s, min)
Ψ	enhancement

Indices—Subscripts

d	dynamic
e	equivalent
g	gas
H	solubility
i	reactant species (generally 1 = SO_2, 2 = O_2 3 = SO_3, 4 = H_2O, 5 = H_2SO_4) reaction index (Table XI)
j	melt component
k	reaction
	complex index (generally 1 = $V_2^{5+}O_2^{2-}$, 2 = $V_2^{5+}O^{2-}$, 3 = $V_2^{5+}SO_3^{2-}$, 4 = V_2^{4+}
L	liquid
l	liquid
m	melt species (Table XIII)
p	particle, constant pressure
R	reaction
s	space time
	solid or particle
	static

in	inactive
	inlet (Table XIII)
evap	evaporation
ext	external
max	maximum
o	time zero condition (Table XI)
3	SO_3

Indices-Superscripts

f	fluid or gas phase (Table XIII)
g	gas
p	particle
L	liquid or melt phase (Table XIII)
m	melt
in	inactive
	inlet (Table XIII)
°	initial or entrance state or condition
+	after time zero, maximum
−	before time zero, maximum
$\bar{3}$	SO_3
$\bar{\ }$	mean

REFERENCES

Balzhinimaev, B. S., Belyeava, N. P., and Ivanov, A. A., Kinetics of dissolution of inactive crystalline phase in vanadium catalysts for SO_2 oxidation. *React. Kinet. Catal. Letters* **29,** 465–472 (1985).

Balzhinimaev, B. S., Ivanov, A. A., Lapinaa, O. B., Mastikhin, M., and Zamaraev, K. I., The mechanism of SO_2 oxidation over supported vanadium catalysts. *Disc. Faraday Chem. Soc.* **87**(8), 1–15 (1989).

Berruti, F., Hudgins, R. R., Rhodes, E., and Sicardi, S., Oxidation of sulfur dioxide in a trickle-bed reactor. A study of reactor modelling. *Can. J. Chem. Eng.* **62,** 644–650 (1984).

Boreskov, G. K., and Matros, Yu. Sh., Unsteady-state performance of heterogeneous catalytic reactions. *Catal. Rev.—Eng. Sci.* **25,** 551–590 (1984).

Boreskov, G. K., Matros, Yu. Sh., Kiselov, O. V., and Bunimovich, G. A., Realization of heterogeneous catalytic processes under unsteady-state conditions. *Dokl. Acad. Nauk USSR* **237,** 160–163 (1977).

Boreskov, G. K., Bunimovich, G. A., Matros, Yu. Sh., and Ivanov, A. A., *Kinet. Catal.* **23,** 402 (1982).

Briggs, J. P., Hudgins, R. R., and Silveston, P. L., Composition cycling of an SO_2 oxidation reactor. *Chem. Eng. Sci.* **32,** 1087–1092 (1977).

Briggs, J. P., Kane, D. M., Hudgins, R. R., and Silveston, P. L., Reduction of SO_2 emissions from an SO_2 converter by means of feed composition cycling to the final stage, *in* "Proc.

1st Intern. Waste Treatment and Utilization Conf." (Moo Young, M. W., and G. Farquhar, Ed.), (Univ. of Waterloo, Waterloo, Ontaro) pp. 521–533, 1978.

Budman, H., Kryzonak, M., and Silveston, P. L., Control of a nonadiabatic packed bed reactor under periodic flow reversal. *Can. J. Chem. Eng.* **74,** 751–759 (1996).

Bunimovich, G. A., Matros, Yu. Sh., and Boreskov, G. K., Unsteady state performance of sulphur dioxide oxidation in production of sulfuric acid. *in* "Frontiers in Chemical Reaction Engineering," Vol. 2 (Doraiswarmy, L. K., and R. A. Mashelkar, Eds.). Wiley Eastern, New Delhi, 1984.

Bunimovich, G. A., Strots, V. O., and Goldman, O. V., Theory and industrial application of SO_2 oxidation reverse-process for sulphuric acid production, *in* "Unsteady-state Processes in Catalysis" (Matros, Yu. Sh., Ed.). VNU Science Press, Utrecht, 1990, pp. 7–24.

Bunimovich, G. A. Vernikovskaya, N. V., Strots, V. O., Balzhinimaev, B. S., and Matros, Yu. Sh., SO_2 oxidation in a reverse-flow reactor: influence of a vanadium catalyst dynamic properties. *Chem. Eng. Sci.* **50,** 565–580 (1995).

Carlsson, L., Sandgren, B., Simonsson, D., and Rihousky, M., Design and performance of a modular, multi-purpose electrochemical reactor. *J. Electrochem. Soc.* **130,** 342–350 (1983).

De Vos, R., Hatziantoniou, V., and Schöön, N.-H., The cross-flow catalyst reactor. An alternative for liquid phase hydrogenations. *Chem. Eng. Sci.* **37,** 1719–1726 (1982).

De Vos, R., Smedler, G., and Schöön, N.-H., Selectivity aspects of using the cross-flow catalyst reactor for liquid phase hydrogenations. *Ind. Eng. Chem. Process Des. Dev.* **25,** 197–202 (1986).

Eigenberger, G., and Nieken, U., Catalytic combustion with periodic flow reversal. *Chem. Eng. Sci.* **43,** 2109–2115 (1988).

Gangwal, S. K., McMichael, W. J., Howe, G. B., Spivey, J. J., and Silveston, P. L., Low-temperature carbon-based process for flue-gas cleanup. *IChemE Symp.* Series, No. 131 (1992).

Hasokowati, W., Hudgins, R. R., and Silveston, P. L., Loading, draining and hold-up in periodically operated trickle-bed reactors. *Can. J. Chem. Eng.* **72,** 405–410 (1994).

Hatziantoniou, V., Andersson, B., and Schöön, N.-H., Mass transfer and selectivity in liquid phase hydrogenation of nitro compounds in a monolithic catalyst reactor with segmented gas–liquid flow. *Ind. Eng. Chem. Process Des. Dev.* **25,** 964–970 (1986).

Haure, P. M., Hudgins, R. R., and Silveston, P. L., Periodic operation of a trickle bed reactor, *AIChEJ.* **35,** 1437–1444 (1989).

Haure, P. M., Bogdashev, S. M., Bunimovich, M., Stegasov, A. N., Hudgins, R. R., and Silveston, P. L., Thermal waves in the periodic operation of a trickle- bed reactor, *Chem. Eng. Sci.* **45,** 2255–2261 (1990).

Haure, P. M., Hudgins, R. R., and Silveston, P. L., Investigation of SO_2 oxidation rates in trickle-bed reactors operating at low liquid flow rates. *Can. J. Chem. Eng.* **70,** 600–603 (1992).

Isozaki, C., Katagiri, T., Nakamura, Y., Hirabayashi, S., Yabe S., and Yamaki, T., Demonstration of DC/DA sulphuric acid plant based on unsteady-state *in* "Unsteady-state Processes in Catalysis" (Matros, Yu. Sh., Ed.). VNU Science Press, Utrecht, 1990, pp. 637–642.

Ivanov, A. A., and Balzhinimaev, B. S., New data on kinetics and reaction mechanism for SO_2 oxidation over vanadium catalysts. *React. Kinet. Catal. Lett.* **35,** 413–424 (1987).

Kirillov, V. A., and Stegasov, A. N., On the simulation of heterogeneous catalytic processes with phase transitions in fixed catalyst bed (in Russian). *Teoreticheskiye osnoy khimicheskoi teknhnologii* **22,** 340–345 (1988).

Kirillov, V. A., Kuzmin, V. A., Pyanov, V. I., and Khanaev, V. M., Analysis of transfer process in a packed bed with concurrent down-flow of gas and liquid. *Hung. J. Ind. Chem.* **11,** 263–274 (1983).

Komiyama, H., and Smith J. M., Sulfur dioxide oxidation in slurries of activated carbon. *AIChEJ.* **21,** 664–676 (1975).

Lee, J.-K., Hudgins, R. R., and Silveston, P. L., A cycled trickle-bed reactor for SO_2 oxidation. *Chem. Eng. Sci.* **50,** 2523–2530 (1995).

Lee, J.-K., Hudgins, R. R., and Silveston, P. L., SO_2 oxidation in a periodically operated trickle-bed comparison of activated carbon catalysts. *Environ. Prog.* **15**(4), 239–244 (1996a).

Lee, J.-K., Ferrero, S., Hudgins, R. R., and Silveston, P. L., Catalytic SO_2 oxidation in a periodically operated trickle-bed: reactor. *Can. J. Chem. Eng.* **74,** 706–712 (1996b).

Mata, A. R., and Smith, J. M., Oxidation of sulfur dioxide in a trickle bed reactor. *Chem. Eng. J.* **22,** 229–235 (1981).

Matros, Yu. Sh., "Unsteady Processes in Catalytic Reactors." Elsevier Science Publishers, Amsterdam, 1985.

Matros, Yu. Sh., Unsteady-state oxidation of sulphur dioxide in sulphuric acid production. *Sulphur* **183,** 23 (1986).

Matros, Yu. Sh., "Catalytic Processes under Unsteady-State Conditions." Elsevier Science Publishers, Amsterdam, 1989.

Matros, Yu. Sh., and Bunimovich, G. A., Reverse-flow operation in fixed bed catalytic reactors. *Catal. Rev.—Sci. Eng.* **38**(1), 1–68 (1996).

Metzinger, J., Hudgins, R. R., Silveston, P. L., Gangwal, S. K., Application of a periodically operated trickle bed to sulfur removal from stack gas. *Chem. Eng. Sci.* **47,** 3723–3727 (1992).

Metzinger, J., Kühter, A., Silveston, P. L., and Gangwal, S. K., Novel periodic reactor for scrubbing SO_2 from industrial stack gases. *Chem. Eng. Sci.* **49,** 4533–4546 (1994).

Morsi, B. I., and Charpentier, J. C., On mass transfer with chemical reaction in multiphase systems. *NATO ASI CESME,* Izmir, Turkey, (1981).

Nieken, U., Kolios, G., and Eigenberger, G., Control of the ignited steady state in autothermal fixed-bed reactors for catalytic combustion. *Chem. Eng. Sci.* **49,** 5507–5518 (1994).

Purwono, S., Budman, H., Hudgins, R. R., Silveston, P. L., and Matros, Yu. Sh., Runaway in packed bed reactors operating with periodic flow reversal. *Chem. Eng. Sci.* **49,** 5473–5487 (1994).

Ramachandran, P. A., and Smith, J. M., Dynamic behavior of trickle bed reactors. *Chem. Eng. Sci.* **34,** 75–91 (1979).

Rao, V. G., and Drinkenburg, A. A. H., A model for pressure drop in two-phase gas-liquid down-flow through packed columns. *AIChEJ.* **31,** 1010–1018 (1985).

Rhee, H.-K., and Amundson, N. R., Equilibrium theory of creeping profiles in fixed-bed catalytic reactors. *Ind. Eng. Chem. Funda.* **13,** 1–4 (1974).

Sapundzhiev, H., Grozev, G., and Elenkov, D., Influence of geometric and thermophysical properties of reaction layer on sulphur dioxide oxidation in transient conditions. *Chem. Eng. Technol.* **13,** 131–135 (1990).

Satterfield, C. N., and Ozel, F., Direct solid-catalyzed reaction of a vapor in an apparently completely wetted trickle bed reactor. *AIChEJ.* **19,** 1259–1261 (1973).

Sedricks, W., and Kenney, C. N., Partial wetting in trickle bed reactors—the reduction of crotonaldehyde over a palladium catalyst. *Chem. Eng. Sci.* **28,** 558–1261 (1973).

Silveston, P. L., and Hudgins, R. R., Reduction of sulfur dioxide emissions from a sulfuric acid plant by means of feed modulation. *Environ. Sci. Technol.* **15,** 419–422 (1981).

Silveston, P. L., Hudgins, R. R., Bogdashev, S., Vernijakovskaja, N and Matros, Yu. Sh., Modelling of a periodically operated packed bed SO_2 oxidation reactor at high conversion in "Unsteady-state Processes in Catalysis (Matros, Yu. Sh., Ed.). VNU Science Press, Utrecht, 1990.

Silveston, P. L., Hudgins, R. R., Bogdashev, S., Vernijakovskaja, N., and Matros, Yu. Sh.,

Modelling of a periodically operated packed bed SO_2 oxidation reactor at high conversion. *Chem. Eng. Sci.* **49**(3), 335–341 (1994).

Snyder, J. D., and Subramaniam, B., Numerical simulation of a periodic flow reversal reactor for sulfur dioxide production. *Chem. Eng. Sci.* **48,** 4051–4064 (1993).

Specchia, V., and Baldi, G., Pressure drop and liquid hold-up for two-phase concurrent flow in packed beds. *Chem. Eng. Sci.* **32,** 515–523 (1977).

Stegasov, A. N., Kirillov, V. A., and Silveston, P. L., Modelling of catalytic SO_2 oxidation for continuous and periodic liquid flow through a trickle bed. *Chem. Eng. Sci.* **49,** 3699–3710 (1992).

Strots, V. O., Matros, Yu. Sh., Bunimovich, G. A., Periodically forced SO_2 oxidation in CSTR. *Chem. Eng. Sci.* **47**(9–11), 2701–2706 (1992).

Tan, C. S., and Smith, J. M. Catalyst particle effectiveness with unsymmetrical boundary conditions. *Chem. Eng. Sci.* **35,** 1601–1609 (1980).

Unni, M. P, Hudgins, R. R., Silveston, P. L., Influence of cycling on the rate of oxidation of SO_2 over a vanadia catalyst. *Can. J. Chem. Eng.* **51,** 623–629 (1973).

Van den Bussche, K. M., Neophytides, S. N., Zolotarskii, I. A., and Froment, G. F., Modelling and simulation of the reverse flow operation of a fixed bedreactor for methanol synthesis. *Chem. Eng. Sci.* **48**(12), 3335–3345 (1993).

Wu, H., Zhang, S., Li, C., and Fu, J., Modeling of unsteady-state oxidation process of SO_2 (I) axial heat transfer of fixed bed packed with vanadium catalyst. *J. Chem. Ind. Eng. (China)* **46,** 416–423 (1995).

Wu, H., Zhang, S., and Li, C., Study of unsteady-state catalytic oxidation of sulphur dioxide by periodic flow reversal. *Can. J. Chem. Eng.* **74,** 766–771 (1996).

Xiao, W.-D., and Yuan, W.-K., Modelling and simulation for adiabatic fixed-bed reactor with flow reversal. *Chem. Eng. Sci.* **49**(21), 3631–3641 (1994).

Xiao, W.-D., and Yuan, W.-K., Modelling and experimental studies on unsteady-state SO_2 converters. *Can. J. Chem. Eng.* **74,** 772–782 (1996).

Yang, M.-C., and Cussler, E. L., A hollow fiber trickle bed reactor. *AIChEJ.* **33,** 1754–1760 (1987).

Zhang, S., Wu, H., and Li, C.-Y., 'Modeling of unsteady-state oxidation process of SO_2 (II)—Model simulation and parameter analysis.' *J. Chem. Ind. Eng.(China)* **46,** 424–430 (1995).